OFFICE OF NAVAL RESEARCH

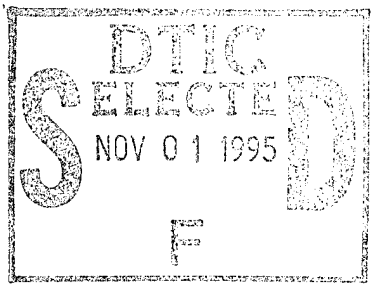


GRANT N00014-92-J-1243 P06

R&T Code 3131065 --06

Technical Report No. 15

# The Quantum Dynamics of an Excess Proton in Water



by

J. Lobaugh and Gregory A. Voth

To Be Submitted

to

Journal of Chemical Physics

University of Pennsylvania
Department of Chemistry
Philadelphia, PA 19104-6323

October 1995

# REPORT DOCUMENTATION PAGE

Form Approved
OMB No. 0704-0188



| 1. AGENCY USE ONLY (Leave blank) | 2. REPORT DATE | 3. REPORT TYPE AND DATES COVERED |
|---|---|---|
| | 10-9-95 | Technical 5/95 - 5/96 |

**4. TITLE AND SUBTITLE**

The Quantum Dynamics of an Excess Proton in Water

**5. FUNDING NUMBERS**

ONR N00014-92-J-1243 P06

R&T Code 3131065---06

**6. AUTHOR(S)**

J. Lobaugh and Gregory A. Voth

**7. PERFORMING ORGANIZATION NAME(S) AND ADDRESS(ES)**

Department of Chemistry
University of Pennsylvania
231 S. 34th Street
Philadelphia, PA 19104-6323

**8. PERFORMING ORGANIZATION REPORT NUMBER**

**9. SPONSORING/MONITORING AGENCY NAME(S) AND ADDRESS(ES)**

Office of Naval Research
Chemistry Division
800 N. Quincy Street
Arlington, VA 22217-5000

**10. SPONSORING/MONITORING AGENCY REPORT NUMBER**

ONR Technical Report #15

**11. SUPPLEMENTARY NOTES**

**12a. DISTRIBUTION/AVAILABILITY STATEMENT**

Approved for public release: distribution unlimited.

**12b. DISTRIBUTION CODE**

**13. ABSTRACT** *(Maximum 200 words)*

The quantum dynamics and energtics of an excess in water have been studied computationally. Comparison of a quantum mechanical treatment of the transferring proton and the water solvent is made with a classical treatment of the same system. The exchange of the proton between two water molecules is found to be an activationless quantum process. Analysis of the microscopic structure of the solvent around the proton transfer complex is also carried out, and the quantum IR spectrum of the transferring proton is calculated and analyzed in terms of Zundel polarization. The Grötthus mechanism for proton migration in water is also examined within the context of the model. Grötthus behavior is suggested to depend critically on the dynamics of water molecules in the second solvation shell of the $H_5O_2^+$ complex, as well as the inward fluctuations of the oxygen-oxygen distance of water molecules that hydrogen bond to the $H_5O_2^+$ complex in the first solvation shell. The quantum effects on the nuclear dynamics are found to be significant.

| 14. SUBJECT TERMS | 15. NUMBER OF PAGES |
|---|---|
| Chemical dynamics; computer simulation; electrochemistry | 55 |
| | 16. PRICE CODE |

| 17. SECURITY CLASSIFICATION OF REPORT | 18. SECURITY CLASSIFICATION OF THIS PAGE | 19. SECURITY CLASSIFICATION OF ABSTRACT | 20. LIMITATION OF ABSTRACT |
|---|---|---|---|
| Unclassified | Unclassified | Unclassified | |

# The Quantum Dynamics of an Excess Proton in Water

J. Lobaugh* and Gregory A. Voth

*Department of Chemistry, University of Pennsylvania, Philadelphia, Pennsylvania 19104-6323*

(August 15, 1995)

## Abstract

The quantum dynamics and energetics of an excess proton in water have been studied computationally. Comparison of a quantum mechanical treatment of the transferring proton and the water solvent is made with a classical treatment of the same system. The exchange of the proton between two water molecules is found to be an activationless quantum process. Analysis of the microscopic structure of the solvent around the proton transfer complex is also carried out, and the quantum IR spectrum of the transferring proton is calculated and analyzed in terms of Zundel polarization. The Grötthus mechanism for proton migration in water is also examined within the context of the model. Grötthus behavior is suggested to depend critically on the dynamics of water molecules in the second solvation shell of the $H_5O_2^+$ complex, as well as the inward fluctuations of the oxygen–oxygen distance of water molecules that hydrogen bond to the $H_5O_2^+$ complex in the first solvation shell. The quantum effects on the nuclear dynamics are found to be significant.

---

*Present Address: Department of Chemistry and Biochemistry, University of Texas at Austin, Austin, TX, 78712-1167

## I. INTRODUCTION

Proton transfer in water has been the focus of considerable theoretical and experimental investigation during this century. A lone proton does not exist in water but instead forms a weak chemical bond with a water molecule to give a hydronium ( $H_3O^+$ ) ion. The mobility of the hydronium itself is anomalously high, being five to seven times that of similarly sized cations [1]. The explanation of this unusual fact is thought to be that the migration of an excess proton in water could occur via a mechanism of *chemical*, rather than hydrodynamic or Stokes' law, diffusion. The positive charge might therefore shuttle through water via an exchange of chemical and hydrogen bonds (as illustrated in Fig. 1), hence the charge migration could occur via a process of structural diffusion, [2] also called the Grötthus mechanism.

A classic variant on this model suggested by Bockris [3,4] is one in which the rate determining step is the molecular reorientation of a water adjacent to the $H_3O^+$ in order to form a hydrogen bond with the $H_3O^+$ ion. One drawback of this theory is that the thermal rate of reorientation of water molecules in pure water is insufficiently fast to account for the rate of proton transfer [3]. However, it can be postulated that the electric field of the hydronium enhances the rate of molecular reorientation. This process is known as "field assisted" reorientation and is could be sufficiently fast to account for the rate of proton transfer [4]. On the other hand, it has been pointed out [5–7] that the activation energy necessary to transfer a proton to an acceptor water that is not hydrogen bonded to other water molecules in the second solvation shell (which is a consequence of the field reorientation mechanism) exceeds the experimentally determined [8] activation energy of proton transfer. Furthermore, the theory as originally put forward [3,4] would seem to require the presence of a second hydronium to perturb the local structure around the first hydronium (see also [9]). In addition, the mobilities of $H^+$ and $OH^-$ are smaller [10] in ice than in water which would seem to contradict a field "assisted" reorientation mechanism. Hence, it seems that the rate limiting step for proton transfer might not involve reorientation dynamics in the first solvation

shell but instead could involve dynamics of water molecules in the second solvation shell of the $H_3O^+$ ion. In this picture, the formation of hydrogen bonds in the second solvation shell with a water molecule in the first solvation shell is a precursor to a Grötthus–type proton transfer event [7,11–13]. Also critical to a successful proton transfer event could be the inward fluctuation of the oxygen–oxygen distance between the hydronium ion and the acceptor water molecule in the first solvation shell [14,15] since the barrier to proton transfer increases rapidly as the oxygen–oxygen distance increases [16–20]. Hence, proton transfer must be a concerted process depending on fluctuations in both the oxygen–oxygen distance between donor and acceptor as well as the nearby solvent dynamics.

The proton due to its small mass can give rise to quantum effects in many chemical reactions (see, e.g., Refs. [21–25]). The thermal DeBroglie wavelength of a proton is $\sim$ 1.0 Å which is of the same magnitude as the length scale over which proton transfer takes place in solution. In addition, the isotope ratios for the rate constants of the chemical reactions $H_2O + H_3O^+ \xrightarrow{k_1} H_3O^+ + H_2O$ and $H_2O + OH^- \xrightarrow{k_2} OH^- + H_2O$ have been measured [26] to be $k_1^H / k_1^D = 1.6 \pm 0.2$ and $k_2^H / k_2^D = 2.7 \pm 0.4$, respectively. The effects are somewhat larger than the kinetic isotope effect $(m_H/m_D)^{1/2}$ which indicates that quantum effects may be present to some degree in both reactions.

The hydronium species [4,11,12] in water has, on the average, $C_{3v}$ symmetry [27] and four water molecules in its first solvation shell [28]. Alternatively, Zundel [29] and others [30] have characterized the excess proton as an $H_5O_2^+$ "grouping" in water in which the excess proton tunnels rapidly back and forth between the two water molecules through the strong hydrogen bond. There is some contention in the literature as to which species predominates in the liquid [27]. A recent pioneering *ab initio* MD study [31] indicates that both viewpoints are in essence correct, at least for classical nuclear dynamics. In this study, it was found that there is a rapid interconversion between the $H_9O_4^+$ and $H_5O_2^+$ structures [32] in solution and this interconversion is governed by the dynamics of the local solvent structure in the second solvation shell of the $H_3O^+$ ion.

*Ab initio* studies of proton transfer in small gas phase water clusters are numerous (see,

e.g., Refs. [6,7,16–20,33–37]). These studies have characterized the $H_5O_2^+$ complex as having a flat and broad potential on which the excess proton moves. The proton potential surface, depending on the level of *ab initio* theory used, is either a single minimum or double minimum with a transition state 0.2–0.5 kcal $mol^{-1}$ higher than the minima. As additional water molecules are added, the potential of the proton becomes a single minimum and shifts according to the number and positioning of water molecules added to the complex [6,7]. In extending this picture to the bulk solvent, it is thought the dynamics of the excess proton is governed by solvent fluctuations about the proton transfer complex. The electric field of the solvent determines, in part, the potential on which the proton moves and induces shifts of the proton from one water molecule to the other. As the proton shifts there is a charge redistribution in the proton transfer complex ( $H_5O_2^+$ ). This charge redistribution is a polarization effect termed "Zundel Polarization" [38–40].

There have been few computational investigations of proton transfer in water using Molecular Dynamics (MD) or Monte Carlo (MC) methods [41–44] because of the difficulty in specifying empirical potential functions that correctly describe proton transfer along a series of hydrogen bonded water molecules. The recent "first–principles" studies of this and related systems [31,45–48] using *ab initio* MD [also known as the Car–Parrinello (CP) method [49–52]] have taken a significant step forward forward on the problem. The CP method is a dynamical density functional theory–based (DFT) method wherein the electronic structure is calculated "on the fly" while being adiabatically "slaved" to the evolving classical nuclei within the Born–Oppenheimer approximation. The forces on the classical nuclei are calculated from the Hellman–Feynman theorem. Hence, chemical processes such as bond breaking or formation are treated at an *ab initio* level rather than using empirical methods and/or potentials, representing a substantial advance in MD simulation capability. Unfortunately, the high computational cost has limited the size of systems studied and prevented the length of the CP simulations from being more than four to five picoseconds, which is often insufficient to obtain well converged values of thermodynamic and dynamical quantities of interest. Moreover, the accuracy of gradient–corrected DFT methods for

describing the proton transfer barrier in the $H_5O_2^+$ complex has been called into question [15], and the nuclei are treated as being classical in the CP simulations.

In the present paper, the dynamical and equilibrium properties of an excess proton are studied via classical MD and Feynman path integral methods. The potential energy modeling is accomplished using a two state Empirical Valence Bond (EVB) [53,54] model for the $H_5O_2^+$ complex in water. The goal of this work is somewhat more modest than an explicit simulation of the Grötthus mechanism: the activation free energy as well as the dynamics of a proton transferring between a hydronium ion and an acceptor water molecule in the first solvation shell are calculated using both the quantum and classical treatments of the system. The quantum effects on the proton exchange along the strong hydrogen bond between the $H_3O^+$ ion and a water molecule are thus examined. From the results presented in the following sections, it will be suggested that the transfer of a proton from a hydronium ion to a neighboring water molecule is not the rate limiting step in the proton migration process. Rather, the likely quantum dynamical mechanism for extended (Grötthus–type) proton transfer can be uncovered by examining the structure and dynamics of the solvent molecules around the proton transfer complex. To our knowledge, the present work is the first quantum simulation of the nuclear dynamics of an excess proton in water.

The sections of this paper are organized as follows: In Sec. II, the computational methods used to simulate the dynamics and energetics of an excess proton in water are outlined. The parameterization of the empirical model is then described in Sec. III, while the results of the quantum and classical simulations are discussed in Sec. IV. Concluding remarks are given in Sec. V.

## II. COMPUTATIONAL METHODS

### A. Path Integral Quantum Transition State Theory

In several previous studies of proton transfer reactions [55–58] the Feynman path integral quantum transition state theory (PI–QTST) approach [59–62] has been used to calculate the quantum mechanical activation free energy of proton transfer. Both solvent and intramolecular contributions to the activation free energy of proton transfer are included in this approach and the method is applicable [63] in both the adiabatic and nonadiabatic limits of proton transfer and where the proton itself becomes classically activated. Importantly, the quantum tunneling of the proton is explicitly included in the calculation. [56,63] The PI–QTST method makes no approximation or assumptions concerning the form of the coupling of the proton transfer coordinate to the solvent and includes the highly nonlinear intramolecular and intermolecular couplings between the proton transfer coordinate and the other molecular modes of the proton transfer complex.

In the PI–QTST formulation, [59–61] the fundamental quantum rate constant for a quantum activated rate process can be written as

$$k \;=\; \kappa \frac{k_B T}{h Q_R} exp(-\beta F_c^*) \quad , \tag{2.1}$$

where $\kappa$ is a quantum dynamical transmission coefficient [59–61] of order unity, $Q_R$ is the partition function of the entire solute–solvent system in its reactant configuration, $k_B$ is Boltzmann's constant, $T$ is the temperature, $\beta$ is $1/k_B T$, and $F_c^*$ is a quantum mechanical excess free energy, given by [59–61]

$$F_c^* \;=\; -\,k_B T\, ln\left[Q_c(q^*)/(\mu/2\pi\hbar^2\beta)^{1/2}\right] \quad . \tag{2.2}$$

The quantity $Q_c(q^*)$ in Eq. 2.2 is the path integral centroid density [59–61,64], given in the case of a proton transfer reaction by [56,63]

$$Q_c(q^*) \;=\; \int\cdots\int \mathcal{D}\mathbf{r}(\tau)\; \mathcal{D}\mathbf{R}(\tau)\; \delta(q^* - \tilde{q}_0)\, exp\{-S[\mathbf{r}(\tau),\mathbf{R}(\tau)]/\hbar\} \quad , \tag{2.3}$$

where the coordinates $\mathbf{r}$ are the Cartesian coordinates of the proton and the coordinates $\mathbf{R}$ are all other general coordinates of the system, including the solvent. The coordinate $q$ is the proton transfer reaction coordinate having a reduced mass $\mu$. The reaction coordinate in the case of $H_2O$–H-$OH_2^+$ complex is the asymmetric stretch mode involving the transferring proton and the two oxygen atoms of the donor and acceptor water molecules, i.e.,

$$q_{asym} = \frac{1}{2}(r_1 - r_2) \quad , \tag{2.4}$$

where $r_1$ and $r_2$ are the distances between the proton (labeled $H_3$ in Fig. 2) and each oxygen atom respectively (labeled $O_1$ and $O_2$ in Fig. 2). The centroid variable of the reaction coordinate path $q(\tau)$ is defined as [59–62,64]

$$\tilde{q}_0 = \frac{1}{\beta\hbar}\int_0^{\beta\hbar} d\tau\, q(\tau) \tag{2.5}$$

and is constrained to be at the transition state between the reactant and product states of the proton [56,63] (which in this case is $q_{asym}$=0). The action $S[\mathbf{r}(\tau), \mathbf{R}(\tau)]$ in Eq. (2.3) is the imaginary time path integral action functional [64], which depends both on the paths of the proton coordinates $\mathbf{r}(\tau)$ and those of the remaining coordinates of the system $\mathbf{R}(\tau)$. The specific expression for the action functional in Eq. (2.3) is given by [64]

$$S[\mathbf{r}(\tau), \mathbf{R}(\tau)] = \int_0^{\beta\hbar} d\tau \left\{ \frac{m_{\mathrm{H}}}{2}\dot{\mathbf{r}}(\tau)^2 + \sum_{i=1}^{N} \frac{M_i}{2}\dot{\mathbf{R}}_i(\tau)^2 + V[\mathbf{r}(\tau), \mathbf{R}(\tau)] \right\} \quad , \tag{2.6}$$

where $V[\mathbf{r}(\tau), \mathbf{R}(\tau)]$ is the general many–body potential. All possible quantum paths of the coordinates are integrated over in the functional integration in Eq. (2.3). The classical approximation for any of the variables $\mathbf{R}$ in Eq. (2.3) is to replace the quantum paths $\mathbf{R}(\tau)$ by their equivalent classical coordinates. Due to the heavy mass of the oxygen atom, the oxygen coordinates were treated classically and so the aforementioned replacement was made for their quantum paths. All of the protons (not just the transferring proton) in the solvent water molecules and transfer complex were treated quantum mechanically in this study.

Equation (2.1) can be written in a form particularly well suited for computer simulation as [56]

$$k = \kappa \frac{\omega_c}{2\pi} exp(-\beta \Delta F_c^*) \quad , \tag{2.7}$$

where $\mu\omega_c^2$ is the curvature of the reaction coordinate centroid free energy around the reactant configurations (i.e., for $\tilde{q}_0$ near $q_r$), the prefactor $\kappa$ is approximated to be unity, and the difference in centroid free energies between the reactant and transition state is given by

$$\begin{aligned} \Delta F_c^* &= -k_B T \, ln[Q_c(q^*)/Q_c(q_r)] \\ &= -k_B T \, ln[P_c(q_r \rightarrow q^*)] \quad . \end{aligned} \tag{2.8}$$

A number of simulation methods are suitable for evaluating path integrals and Eq. (2.8). In the case of high barriers, one method is to sample the classical coordinates and the path integral quasiparticle coordinates using Path Integral Monte Carlo (PIMC) [65–69] or Path Integral Molecular Dynamics (PIMD) [70] with umbrella sampling [71]. However, since the activation energy of proton transfer is quite low (on the order of $k_B T$) in this particular study, the probability $P_c(q_r \rightarrow q^*)$ is readily calculated by binning the trajectory of the centroid of the reaction coordinate as it evolves unconstrained (i.e. without the influence of an umbrella potential) during the simulation. The PIMD method was chosen to simulate the proton transfer system in this study. In this method, the primitive representation of the discretized path integral action functional is used so that each quantum particle maps onto an isomorphic polymer "necklace" consisting of $P$ quasiparticles, held together by harmonic springs [72,73]. The partition function in a notation specific to the proton transfer complex and the accompanying system of water molecules is given by

$$Q_P = \left(\frac{m_{\mathrm{H}} P}{2\beta^2\hbar^2}\right)^{3(N_{\mathrm{H}}+1)P/2} \left(\frac{m_{\mathrm{O}}}{2\beta^2\hbar^2}\right)^{3N_{\mathrm{O}}/2} \prod_{i=1}^{P} \left(\prod_{j=1}^{N_{\mathrm{H}}} d\mathbf{R}_{\mathrm{H}_j}^{(i)}\right) d\mathbf{r}^{(i)} \prod_{j=1}^{N_{\mathrm{O}}} d\mathbf{R}_{\mathrm{O}_j} \exp\left(-\beta V_P\right) \tag{2.9}$$

where the proton (oxygen) coordinates of the water solvent as well as donor and acceptor waters are denoted by $\mathbf{R}_{\mathrm{H}}(\mathbf{R}_{\mathrm{O}})$. The proton (oxygen) mass is $m_{\mathrm{H}}$ ($m_{\mathrm{O}}$). The coordinates of the transferring proton are denoted by $\mathbf{r}$. The potential $V_P$ in Eq. (2.9) is given by

$$\begin{aligned} V_P = &\frac{P m_{\mathrm{H}}}{2\hbar^2\beta^2} \sum_{i=1}^{P} \sum_{j=1}^{N_{\mathrm{H}}} \left(\mathbf{R}_{\mathrm{H}_j}^{(i+1)} - \mathbf{R}_{\mathrm{H}_j}^{(i)}\right)^2 + \left(\mathbf{r}^{(i+1)} - \mathbf{r}^{(i)}\right)^2 \\ &+ \frac{1}{P} \sum_{i=1}^{P} V\left(\mathbf{R}_{\mathrm{H}_1}^{(i)}, ..., \mathbf{R}_{\mathrm{H}_{N_{\mathrm{H}}}}^{(i)}; \mathbf{r}^{(i)}; \mathbf{R}_{\mathrm{O}_1}, ..., \mathbf{R}_{\mathrm{O}_{N_{\mathrm{O}}}}\right), \end{aligned} \tag{2.10}$$

and consists of two terms. The first term contains the harmonic springs for the path integral coordinates which are just the kinetic energy terms of Eq. (2.6). The second term is the many–body potential which includes all the intermolecular and intramolecular interactions and is evaluated at $P$ discrete imaginary time slices. The partition function $Q_P$ can be evaluated as an effective classical partition function by introducing fictitious momenta for the quasiparticles and oxygen atoms and using molecular dynamics [70]. The effective Hamiltonian is thus given by

$$H' = \sum_{i=1}^{P} \left( \sum_{j}^{N_{\rm H}} \frac{1}{2} m_{\rm H}^{*} \mathbf{V}_{{\rm H}_j}^{(i)\,2} + \frac{1}{2} m_{\rm H}^{*} \mathbf{v}_{\rm H}^{(i)\,2} \right) + \sum_{j=1}^{N_{\rm O}} \frac{1}{2} m_{\rm O} \mathbf{V}_{{\rm O}_j}^{2} + V_P \tag{2.11}$$

where $m_{\rm H}^{*}$ is the fictitious mass of the proton quasiparticles and $m_{\rm O}$ is the mass of the oxygen nuclei. The velocities of the proton quasiparticles and classical oxygen nuclei are given by $\mathbf{V}_{\rm H}^{(i)}$ and $\mathbf{V}_{\rm O}$, respectively, while that for the transferring proton quasiparticles are given by $\mathbf{v}_{\rm H}^{(i)}$.

### B. Proton Quantum Dynamics

The calculation of quantum dynamical properties for many–body systems with many quantum degrees of freedom is problematical. A number of techniques for computing quantum dynamics are available such as semiclassical methods [74–80] or nonadiabatic dynamics [81–87]. However, none of these methods are particularly useful where a large fraction of the total nuclei must be quantized. A recently developed method known as "Centroid Molecular Dynamics" (CMD) [88–91] which is capable of dealing with such problems will be used in the present study to simulate the dynamics of the proton transfer in a quantized water solvent. The focus of the latter method is on the path centroid as a quasi–classical dynamical variable. The centroid of any proton is defined in Eq. (2.5) and in the discrete representation is written as

$$\mathbf{R}_{\rm H}^{(c)} = \frac{1}{\beta\hbar} \int_0^{\beta\hbar} d\tau\, \mathbf{R}_{\rm H}(\tau) = \frac{1}{P} \sum_{i=1}^{P} \mathbf{R}_{\rm H}^{(i)}, \tag{2.12}$$

where $\mathbf{R}_{\mathrm{H}}(\tau)$ is the Cartesian imaginary time paths of the protons and $\mathbf{R}_{\mathrm{H}}^{(i)}$ are the Cartesian coordinates of the proton quasiparticles. [92]

Associated with the centroid variable is the path integral centroid density, denoted by $\rho_c\left(\mathbf{R}_{\mathrm{H}_1}^{(c)},...,\mathbf{R}_{\mathrm{H}_{N_{\mathrm{H}}}}^{(c)};\mathbf{r}^{(c)};\mathbf{R}_{\mathrm{O}_1},...,\mathbf{R}_{\mathrm{O}_{N_{\mathrm{O}}}}\right)$ in the present case. This equilibrium density, which bears the closest resemblance to the classical Boltzmann density, is formally calculated by fixing the centroid variables in Eq. (2.12) and then integrating over all configurations of the discretized quasiparticles, subject to a weighting by their effective Boltzmann–like configurational factor. While the centroid picture in equilibrium statistical mechanics is interesting in its own right [93–97], it was the discovery [88,89] and subsequent proof [90] of the classical–like dynamical properties of the centroid variable that have made the present study possible.

The basic notion of CMD is that the position or velocity correlation function for quantum particles in a many–body system can be approximately related to a centroid position or velocity correlation function obtained by running classical–like trajectories on the effective quantum centroid potential [88,96,89–91,97]. The centroid trajectories, as well as the trajectories of any classical degrees of freedom such as the oxygens, are generated by the classical–like MD equations

$$\mathbf{m}_{\mathrm{H}} \cdot \ddot{\mathbf{R}}_{\mathrm{H}}^{(c)}(t) = \mathbf{F}_{\mathrm{H}}^{(c)}\left(\mathbf{R}_{\mathrm{H}}^{(c)},\mathbf{R}_{\mathrm{O}}\right), \tag{2.13}$$

and

$$\mathbf{m}_{\mathrm{O}} \cdot \ddot{\mathbf{R}}_{\mathrm{O}}(t) = \mathbf{F}_{\mathrm{O}}^{(c)}\left(\mathbf{R}_{\mathrm{H}}^{(c)},\mathbf{R}_{\mathrm{O}}\right), \tag{2.14}$$

where the terms $\mathbf{m}_{\mathrm{O}}$ and $\mathbf{m}_{\mathrm{H}}$ are vectors with components $m_{\mathrm{O}}$ and $m_{\mathrm{H}}$. The effective centroid potential $V^{(c)}$ is formally defined as

$$V^{(c)}(\mathbf{R}_{\mathrm{H}}^{(c)},\mathbf{R}_{\mathrm{O}}) = -k_B T \ln\left[\rho_c\left(\mathbf{R}_{\mathrm{H}}^{(c)},\mathbf{R}_{\mathrm{O}}\right)\right]. \tag{2.15}$$

The centroid density in the discrete representation is simply given by

$$\rho_c\left(\mathbf{R}_{\mathrm{H}}^{(c)},\mathbf{R}_{\mathrm{O}}\right) = \int\cdots\int \prod_{i=1}^{P} d\mathbf{R}_{\mathrm{H}}^{(i)}\,\delta\left(\mathbf{R}_{\mathrm{H}}^{(c)} - \mathbf{R}_{\mathrm{H}}^{0}\right)\exp\left\{-\beta V_P\right\}. \tag{2.16}$$

The centroid forces ($\mathbf{F}_{\mathrm{H}}^{(c)}$) on the protonic degrees of freedom in the discretized representation are given by

$$\mathbf{F}_{\mathrm{H}}^{(c)} = -\frac{\int\cdots\int\prod_{i=1}^{P} d\mathbf{R}_{\mathrm{H}}^{(i)}\,\delta\left(\mathbf{R}_{\mathrm{H}}^{(c)} - \mathbf{R}_{\mathrm{H}}^{0}\right)\mathbf{V'}_{\mathrm{H}}\exp\left\{-\beta V_P\right\}}{\int\cdots\int\prod_{i=1}^{P} d\mathbf{R}_{\mathrm{H}}^{(i)}\,\delta\left(\mathbf{R}_{\mathrm{H}}^{(c)} - \mathbf{R}_{\mathrm{H}}^{0}\right)\exp\left\{-\beta V_P\right\}}\ , \tag{2.17}$$

where, from the cyclic invariance of the trace,

$$\mathbf{V'}_{\mathrm{H}} = \frac{1}{P}\sum_{i=1}^{P}\vec{\nabla}_{\mathbf{R}_{\mathrm{H}}^{(i)}} V\left(\mathbf{R}_{\mathrm{H}}^{(i)}, \mathbf{R}_{\mathrm{O}}\right). \tag{2.18}$$

Similarly, the forces for the classical degrees of freedom ($\mathbf{F}_{\mathrm{O}}$) are given by

$$\mathbf{F}_{\mathrm{O}} = -\frac{\int\cdots\int\prod_{i=1}^{P} d\mathbf{R}_{\mathrm{H}}^{(i)}\,\delta\left(\mathbf{R}_{\mathrm{H}}^{(c)} - \mathbf{R}_{\mathrm{H}}^{0}\right)\mathbf{V'}_{\mathrm{O}}\exp\left\{-\beta V_P\right\}}{\int\cdots\int\prod_{i=1}^{P} d\mathbf{R}_{\mathrm{H}}^{(i)}\,\delta\left(\mathbf{R}_{\mathrm{H}}^{(c)} - \mathbf{R}_{\mathrm{H}}^{0}\right)\exp\left\{-\beta V_P\right\}}\ , \tag{2.19}$$

where

$$\mathbf{V'}_{\mathrm{O}} = \frac{1}{P}\sum_{i=1}^{P}\vec{\nabla}_{\mathbf{R}_{\mathrm{O}}} V\left(\mathbf{R}_{\mathrm{H}}^{(i)}, \mathbf{R}_{\mathrm{O}}\right). \tag{2.20}$$

The CMD method includes the effects of quantum zero–point energy and tunneling in molecular dynamics simulations directly and efficiently. While the method is approximate, the supporting results are quite compelling. For example, CMD has proven to be very accurate in several simulations [88,96,89–91,98] and it has been justified through a direct mathematical analysis [90], as well as from a variational perspective [88,96]. Furthermore, when barriers are encountered by the centroid trajectories, the insights from the earlier PI–QTST [59–62] confirm that the trajectories will overcome such barriers with the accurate quantum probability.

## III. MODEL PARAMETERIZATION

### A. $H_5O_2^+$ dimer parameterization

An important issue, of course, is the way in which to model the interactions of a hydronium with a given water molecule in the first solvation shell. To this end, the ground state electronic surface on which the proton transfers between two water molecules was described

using the EVB method [53,54]. In this method, two distinct diabatic electronic states are used (cf. Fig. 3) in which the proton is bound to one water molecule in the first state ($V_{11}$) and to the other water molecule in the second state ($V_{22}$). Empirical potentials were used for the stable hydronium states, while information from explicit electronic structure calculations was used to determine the off–diagonal matrix elements which allow the transitions between the diabatic valence bond states.

To be more specific, the two valence bond states interact through an off–diagonal matrix element $V_{12}$ which can be parameterized as a function of a subset of the nuclear coordinates. The adiabatic ground state potential energy function ($V_{ad}$) for the system nuclei of this simple dimer is found by diagonalizing the 2×2 EVB matrix at each configuration, i.e.,

$$V_{ad} = \frac{1}{2}\left(V_{11} + V_{22}\right) - \frac{1}{2}\sqrt{\left(V_{11} - V_{22}\right)^2 + 4V_{12}^2}. \tag{3.1}$$

In this expression, the empirical potential for a given diabatic state $i$ is written as

$$V_{ii} = V_{intra}^{H_3O^+} + V_{intra}^{H_2O} + V_{pair} \tag{3.2}$$

where $V_{pair}$ is the intermolecular interaction between the water molecule and hydronium ion and $V_{intra}^{H_2O}$ ($V_{intra}^{H_3O^+}$) is the intramolecular potential of the water (hydronium). The intramolecular potential for the hydronium was composed of the three harmonic OH bonds ($r_{OH_i}$) and three HOH angle-bend ($\theta_i$) terms given by,

$$V_{intra}^{H_3O^+} = \sum_{i=1}^{3} k_{OH}\left(r_{OH_i} - r_0\right)^2 + k_\theta\left(\theta_i - \theta_0\right)^2. \tag{3.3}$$

The equilibrium bond length ($r_0$), bond angle ($\theta_0$), and force constants ($k_{OH}$ and $k_\theta$) were chosen to reproduce the four distinct vibrational frequencies of the hydronium ion. The two low frequency bend modes $\nu_4$ and $\nu_2$ of the model were adjusted to reproduce the aqueous phase values of 1730 $cm^{-1}$ and 1200 $cm^{-1}$ [27]. The two high frequency symmetric ($\nu_1$) and asymmetric ($\nu_3$) stretches were adjusted to match the experimental gas phase values of 3650 $cm^{-1}$ and 3730 $cm^{-1}$ [99] since these are more decoupled from the condensed phase effects. The resulting normal modes, as well as the experimental gas phase vibrational frequencies are listed in Table I. The parameters for the dimer model are given in Table II.

The intramolecular potential for the "acceptor" water molecule was the harmonic parameterization of Kutchiso and Morino [100] which is given by [101]

$$V_{intra}^{H_2O} = \sum_{i=1}^{2} \rho_w^2 D_w \left(b_{OH_i} - b_{OH_{eq}}\right)^2 + \frac{1}{2} b \left(b_{HH} - b_{HH_{eq}}\right)^2 + c\left(b_{OH_1} + b_{OH_2} - 2b_{OH_{eq}}\right)\left(b_{HH} - b_{HH_{eq}}\right) + d\left(b_{OH_1} - b_{OH_{eq}}\right)\left(b_{OH_2} - b_{OH_{eq}}\right), \tag{3.4}$$

where $b_{12}$ in the bond length between atoms 1 and 2. The equilibrium bond lengths are given in Table II. The intermolecular interactions between the water molecule and the hydronium ion were taken to be pairwise Lennard–Jones (LJ) and Coulomb interactions between the various ionic sites. These interactions may be written as

$$V_{pair} = 4\epsilon \left[\left(\frac{\sigma}{R_{OO}}\right)^{12} - \left(\frac{\sigma}{R_{OO}}\right)^{6}\right] + \sum_m \sum_n \frac{q_m q_n}{R_{mn}}, \tag{3.5}$$

where $\epsilon$ and $\sigma$ are the usual LJ parameters and $q_m$ ($q_n$) are the partial charges on the $m$th ($n$th) atom of the hydronium (water). The LJ interactions are only between the oxygen atoms. The partial charges were taken from the Mulliken charge population analysis in the gas phase density functional electronic structure calculation of Wei and Salahub [102] for the $H_5O_2^+$ complex. The partial charges, as well as the LJ parameters, are listed in Table III.

As stated previously, the barrier in $H_5O_2^+$ is low to nonexistent in the gas phase, depending on the O–O distance. The off–diagonal term which couples the diabatic states was parameterized to, in part, reproduce this barrier. The parametric form for $V_{12}$ was chosen to be given by

$$V_{12} = V_{12}^0 \exp\left[-\alpha_{OO}\left(R_{OO} - R_{OO}^0\right)^2\right], \tag{3.6}$$

where $V_{12}^0$ is 65.89 kcal mol$^{-1}$, $\alpha_{OO}$ is 8 Å$^{-2}$ and $R_{OO}^0$ is 2.6 Å. This parameterization yields a $V_{ad}$ in Eq. (3.1) that reproduces reasonably well the gas phase *ab initio* potential energy surface of Tortonda, et al. [36]. The potential surface of the latter study was generated by calculating the *ab initio* potential energy at constrained OO and OH distances while allowing for relaxation of all the other coordinates of the complex to their potential energy minimum.

The analogous surface was generated for the empirical potential energy function in Eq. (3.1) through a MC annealing calculation while constraining the same coordinates. The resulting potential surface is shown in Figure 4. The relative separation of the minima and height of the transition state are in good agreement with results of the electronic structure calculation. The height of the barrier is approximately 0.35 kcal $mol^{-1}$ which compares well with the barrier of 0.3 kcal $mole^{-1}$ calculated by Tortonda, et al. [36], though the equilibrium O–O separation is somewhat larger in agreement with the *ab initio* MD result of Tuckerman, et al. [45]

### B. Solvent– $H_5O_2^+$ Complex Interactions

The usual approach in the EVB method is to add the complex–solvent interactions directly to each diabatic state $V_{11}$ and $V_{22}$ in Eq. (3.2). The potential for the entire solvent + solute system is then found by diagonalizing the 2×2 diabatic matrix. An alternative approach is taken here. The gas phase adiabatic surface of Eq. 3.1 is assumed to be a good description of the intramolecular degrees of freedom of the complex and relatively unaffected by the solvent. Hence the adiabatic state of the solute is a function of the solute coordinates alone and does not depend on the solvent. The total potential energy including the solvent–solvent and solvent–complex interactions is thereby written as

$$V = V_{ad} + V_{SS}\left(\mathbf{R}_{\mathrm{H}}, \mathbf{R}_{\mathrm{O}}\right) + V_{SC}\left(\mathbf{R}_{\mathrm{H}}, \mathbf{R}_{\mathrm{O}}, \mathbf{r}\right), \tag{3.7}$$

where $V_{SS}$ contains the solvent–solvent interactions as well as the intramolecular potential energy of the solvent molecules. The term $V_{SC}$ is the potential energy of the solvent–complex coupling. For the water solvent, the SPC water model [103] with the intramolecular harmonic parameterization of Kutchiso and Morino [100,101] was used [cf. Eq. (3.4)]. The equilibrium and dynamical properties of the quantized SPC/F water model will be fully explored in a future publication [104].

As the excess proton transfers between two molecular water hosts, there is considerable redistribution of charge as the net unit positive charge shifts its distribution over the donor

hydronium to the acceptor water. In order to mimic this charge redistribution, the electrostatic atomic site charges of the complex were parameterized as functions of the reaction coordinate, the asymmetric stretch of the transferring proton [cf. Eq. (2.4)]. To this end, the *ab initio* study of Wei and Salahub [102] was used for parameterizing the partial charges of the $H_5O_2^+$ complex with which the solvent interacts. In the latter study, a Mulliken charge population analysis was carried out for all the atoms of the $H_5O_2^+$ complex and charges were calculated at different positions along the proton transfer reaction coordinate. The dependence of these charges on the reaction coordinate was thus reproduced in the empirical model. The following equations were used to reproduce the charge variation. Using the atomic site labeling in Fig. 2, the partial charges for the protons of the complex were given by

$$e_{H_1} = e_H^{H_3O^+} f(q_{asym}) + e_H^{H_2O} [1 - f(q_{asym})], \tag{3.8}$$

$$e_{H_2} = e_H^{H_3O^+} f(q_{asym}) + e_H^{H_2O} [1 - f(q_{asym})], \tag{3.9}$$

$$e_{H_3} = g(q_{asym}), \tag{3.10}$$

$$e_{H_4} = e_H^{H_2O} f(q_{asym}) + e_H^{H_3O^+} [1 - f(q_{asym})], \tag{3.11}$$

$$e_{H_5} = e_H^{H_2O} f(q_{asym}) + e_H^{H_3O^+} [1 - f(q_{asym})]. \tag{3.12}$$

The Coulomb charges of the oxygens were given by

$$e_{O_1} = e_O^{H_3O^+} f(q_{asym}) + e_O^{H_2O} [1 - f(q_{asym})] + \frac{1}{2} [e_{Ht} - g(q_{asym})], \tag{3.13}$$

$$e_{O_2} = e_O^{H_2O} f(q_{asym}) + e_O^{H_3O^+} [1 - f(q_{asym})] + \frac{1}{2} [e_{Ht} - g(q_{asym})]. \tag{3.14}$$

The two charge switching functions $f(q_{asym})$ and $g(q_{asym})$ were given by

$$f(q_{asym}) = \frac{1}{2} [1 - \tanh(q_{asym}/q_{sw})], \tag{3.15}$$

and

$$g(q_{asym}) = -\alpha_{sw} q_{asym}^4 + q_{min}^H. \tag{3.16}$$

The parameters used in the above equations are given in Table IV. The above empirical equations and *ab initio* charges of Wei and Salahub are plotted as a function of the asymmetric stretch coordinate in Fig. 5.

### C. Simulation Details

The discretized partition function $Q_P$ in Eq. (2.9) converges rigorously to the quantum limit as $P \rightarrow \infty$. However, in practice a finite value of $P$ is used so that the thermodynamic properties of interest are sufficiently converged to their quantum value. In the present case, a MC study was performed to select a suitable value of $P$ [104,105]. This study followed along the lines of one suggested by Kuharski and Rossky [106]: It consisted of two solvent water molecules which interacted using the harmonic SPC/F potential (described in Sec. III B) and an additional quadratic potential between their centers of mass. This potential had a minimum at 2.85 Å and a frequency $\omega = 26$ ps$^{-1}$, creating an environment similar to the bulk solvent and typical of water librational motion. A total of $10^6$ trial MC moves were carried out and a number of different properties were examined as a function of $P$ including radial distribution functions and the average intramolecular energy. The value $P = 25$ was found to yield sufficient convergence for these properties.

The fictitious mass $m_{\mathrm{H}}^*$ for the PIMD algorithm based on Eq. (2.11) should be chosen to be as small as possible in order to effect rapid sampling. However, if it is too small, ergodicity problems will occur and/or numerical integration of the equations of motion will be difficult due to the small time step necessary to integrate the high frequency motion of the proton quasiparticles. As a result, the fictitious mass was chosen by a normal mode analysis of a single quantized water molecule with the harmonic intramolecular SPC/F potential and $P = 25$. The mass $m_{\mathrm{H}}^*$ was set to 200 au so that the highest frequency mode was below 6000 cm$^{-1}$.

The Velocity Verlet MD [107] method with an implicit iterative algorithm described by Tuckerman, et al. [108,109] was used to integrate the PIMD Hamiltonian. Two Nosé–Hoover

oscillators [110–112] were used for equilibration, one "attached" to the oxygens, the other to the hydrogen quasiparticles. It was verified that these two Nosé oscillators were sufficient to overcome ergodicity problems associated with PIMD calculations [113]. The Nosé masses ($Q_{\eta_O}$ for the oxygens and $Q_{\eta_H}$ for the protons) were chosen to be [114]

$$Q_{\eta_O} = \frac{3N_O - 3}{\omega_{wat}^2 \beta} \tag{3.17a}$$

$$Q_{\eta_H} = \frac{3PN_H}{\omega_{hyd}^2 \beta} \tag{3.17b}$$

where $\omega_{wat}$ and $\omega_{hyd}$ are the characteristic frequencies of the system and were set to $\omega_{wat}$=680 cm$^{-1}$ and $\omega_{hyd}$=3600 cm$^{-1}$ if the protons were treated classically or $\omega_{hyd} = \sqrt{m_H P / m_H^* \hbar^2 \beta^2}$ if the protons were treated quantum mechanically. The time step used for both the classical and PIMD simulations was 0.5 fs.

### D. Centroid Molecular Dynamics Algorithm

A number of algorithms for solving the CMD equations [cf. Eqs. (2.13)–(2.17)] have been developed [91]. This task is not entirely trivial since the centroid potential $V^{(c)}(\mathbf{R}_H^{(c)}, \mathbf{R}_O)$ is actually a quantum potential of mean force, requiring path integral averaging to find the centroid force at each time step [cf. Eqs. (2.16)–(2.17)]. In the approach taken here the "natural" CMD time step was broken into $N_{MD}$ smaller time steps. At each of these small time steps a PIMD calculation was run to obtain the centroid force. The centroid forces are the forces felt by the centroids of the quantum degrees of freedom and the positions of the classical degrees of freedom. Hence, the PIMD calculation was run with constraints on the Cartesian positions of the centroids [115] without moving the classical degrees of freedom. The forces were averaged over a reasonable number of PIMD time steps followed by a MD move of the proton centroids and the classical oxygen coordinates. This "on the fly" algorithm provides a feasible alternative to a brute force approach for obtaining the centroid force. The CMD time step used was 0.05 fs and the PIMD time step used was 0.5 fs. The centroid force was averaged over five PIMD time steps (e.g., five PIMD timesteps

were used for every CMD time step). The simulations were run at 300 K with 125 molecules (123 water molecules and the $H_5O_2^+$ complex) at the density of water (1.00 g/mL). The interactions were tapered at half the box length with a smooth spherical cutoff.

## IV. RESULTS

### A. Radial Distribution Functions

The microscopic structure of the solvent around the $H_5O_2^+$ complex was first analyzed using radial distribution functions. In Fig. 6, the radial distribution of oxygens about each oxygen of the complex shows a sharp maximum at 2.5 Å. The positioning of the peak is in agreement with the experimental thermal neutron and X-ray scattering studies of Triolo, et al. [28]. If one regards the $H_3O^+$ as a chemically distinct species, the maximum corresponds to the three water molecules that hydrogen bond to the three hydrogens of the $H_3O^+$ in the $H_9O_4^+$ complex. The peak is moved in and sharper than the oxygen–oxygen peak of liquid water which is shown for comparison. However, the peak is split in this case because one of the three oxygens is not a water oxygen but a companion oxygen in the $H_5O_2^+$ complex which is somewhat closer than the oxygens of the two water molecules that hydrogen bond to a given oxygen in the $H_5O_2^+$ complex. This splitting was also seen in *ab initio* simulations of Tuckerman, et al. [31]. In the latter simulations, two different radial distributions were calculated. In the first simulation no splitting was observed which corresponded to the symmetrical $H_9O_4^+$ structure in water. In the second distribution function the peak was split, indicating that one of the water molecules was moved in and the $H_5O_2^+$ complex was present. Since the distribution functions are averaged over very long time intervals in the present study the first peak is split as the two structures interchange. It should be noted that the charge switching parameterization of the empirical model allows the acceptor water to have a charge distribution which is almost the same as that of SPC/F water when the transferring proton is close to the donor hydronium. In addition, the model is parameterized

in such a way that the charge distribution of the donor hydronium is symmetrical over the three atoms of the $H_3O^+$ . These features allow for the dynamical interchange of the $H_9O_4^+$ structure and the $H_5O_2^+$ complex. Both of these were in fact observed in the present simulations using computer visualization packages. The splitting is enhanced in the quantum case because the average oxygen–oxygen distance is greater for the two water molecules that hydrogen bond to the oxygen of the complex. This is due to the fact the average OH bond length of the four hydrogens that do not participate in proton transfer in the $H_5O_2^+$ complex is greater in the quantum case. The OH bond length is $1.048 \pm 0.002$ Å in the classical and $1.068 \pm 0.001$ Å in the quantum case. The average OO distance of the oxygens in the $H_5O_2^+$ complex is $2.4862 \pm 0.0007$ in the classical and $2.4860 \pm 0.0006$ in the quantum cases. Both numbers are in good agreement with the experimentally observed distance of 2.5 Å [28]. The coordination number at the first minimum of the oxygen–oxygen radial distribution is 3.3, while the experimentally determined coordination number is four [28]. It should be noted, however, that the coordination number for the oxygen in the $H_3O^+$ at the minimum of the oxygen–oxygen radial distribution for liquid water ($\sim$ 3.3 Å) is four. Therefore, the coordination number of the $H_3O^+$ when evaluated at the first solvation shell radius of liquid water is more in accord with experiment.

Further insight into the microscopic structure of the solvent can be gained by examining the distribution of hydrogens with respect to the oxygens of the complex (cf. Fig. 7). The transferring proton has been included in this distribution function, but the four hydrogens covalently bound to the complex have not. In the classical treatment of the protons, the peak due to the transferring proton is distributed between 1.0 and 1.5 Å and is split due to the fact that there is a small effective barrier (double well potential) along the proton transfer coordinate. In the quantum case, the peak is not split due to the fact that the proton tunnels and has a large zero point energy above the classical gas phase barrier (cf. the following section). The peak at 1.9 Å present in the water OH distribution function is not present in the hydronium case, indicating that the protons of the waters in the first solvation shell are oriented outwards with respect to the complex. The *classical* distribution

function calculated here is *quantitatively* the same as that found by Tuckerman, et al. [31] using *ab initio* molecular dynamics, although the statistical error is much greater in the *ab initio* simulation. This confirms that the parameterization of the empirical model is quite successful when compared with more sophisticated, but much more costly, dynamical electronic structure methods. The present result also indicates that the quantum effects for the transferring proton are significant, qualitatively changing the distribution function.

The distribution function of the transferring proton with the protons of the complex and protons of the nearby water molecules shows a large maximum corresponding to the four protons of the complex (cf. Fig. 8). Again, the peak is split in the classical case due to the barrier along the proton transfer coordinate. The distribution shows enhanced ordering of the solvent at longer distances due to the overall charge of the complex which aligns the solvent water molecules. All of the radial distribution functions discussed above were averaged over 600 ps.

### B. Asymmetric Stretch Trajectories

Representative trajectories of the proton transfer asymmetric stretch coordinate are shown in Fig. 9, wher the classical (Fig. 9a) and centroid (Fig. 9b) trajectories of the asymmetric stretch coordinate are plotted as functions of time. The high frequency oscillations of the quantum centroid trajectory are of larger amplitude than those of the classical variable. In addition, the classical transfer coordinate sometimes resides on either side of the classical transition state ($q_{asym} = 0$) whereas the centroid trajectory samples the entire range of $q_{asym}$ in smooth fashion, indicating a lower or non–existent activation free energy along the proton transfer coordinate in the quantum case. In the classical case, the value of $q_{asym}$ corresponds to the case of the $H_9O_4^+$ structure about sixty percent of the time and to the $H_5O_2^+$ complex, in which the proton resonates between water molecules, around forty percent of the time. This classical result is again in qualitative agreement with the *ab initio* MD results of Tuckerman, et al. [31] for classical nuclear dynamics, but the effects of nuclear

quantization are again seen to be large in the present study.

### C. Quantum Dynamics of Proton Migration

The activation energy of proton transfer in the $H_5O_2^+$ complex was calculated in both the classical TST (i.e. all the protons in the system were classical) and the quantum PI–QTST. As can be seen from Fig. 10, in the classical limit the activation energy is about 0.51 kcal $mol^{-1}$, which is approximately 0.9 $k_BT$, and arises from the solvent orientational polarization reorganization. There is no centroid activation free energy in the quantum case. The dependence of the activation free energy on system size was also checked; curves for both 123 and 510 water molecules are shown in Fig. 10. Proton "sharing" between two water molecules in the quantized $H_5O_2^+$ complex is clearly an activationless or nearly activationless process and certainly not the rate limiting step to proton migration in water. This result could have been predicted from the character of the centroid trajectory in Fig. 10b.

Interestingly, the activation energy of the rate limiting step for proton transfer in water has been measured in $^{17}O$ experiments by Luz and Meiboom [8] to be approximately 2.4 kcal $mol^{-1}$. Furthermore, the mean residence time of a proton with a given water molecule is around 1.5 ps [8,9,13]. The inverse of this number is the rate of proton transfer and is 0.69 $ps^{-1}$ [8]. The rate is clearly much smaller than the rate of proton transfer through the strong hydrogen bond in the $H_5O_2^+$ complex as evidenced by Fig. 9b. Extended proton migration must therefore occur in a concerted fashion, perhaps requiring both the correct solvent fluctuations in the second solvation shell of the $H_5O_2^+$ complex and an inward fluctuation of the oxygen–oxygen distance between the complex and another water molecule (i.e., the coordinate $R_c$ in Fig. 2). The inward fluctuation of this oxygen–oxygen distance creates a "special" bond wherein the resonating proton "flips" its identity (i.e., from proton three to proton four in Fig. 2), thus forming a new $H_5O_2^+$ complex which includes the inward fluctuating water molecule. It is this switching of the "special" resonating proton hydrogen bond between pairs of oxygen atoms that could give rise to the Grötthus–type

proton migration mechanism. [45]

In order to gain better insight into this process, the rate of inward OO fluctuations of the four waters closest to the $H_5O_2^+$ complex was calculated. This rate was also correlated with the probability that the four water molecules were sufficiently hydrogen bonded to other water molecules. Both conditions are necessary for a flip of the "special" bond to occur and thus for extended proton transfer to occur. In order to define the energy criterion of a hydrogen bond between a water in the first solvation shell of the $H_5O_2^+$ complex and the nearby solvent molecules, the distribution of pairwise energies was calculated for the four waters closest to the $H_5O_2^+$ complex with the other water molecules of the solvent. The classical and quantum distributions are shown in Fig. 11. The hump on the shoulder of the distribution is due to hydrogen bonding.

The rate of inward oxygen–oxygen fluctuations was calculated by first "tagging" the four water molecules closest to the oxygen–oxygen complex. A dividing surface was placed at a distance $R_c$ and the rate at which the oxygen–oxygen distance crossed the dividing surface was measured. A crossing of the dividing of the surface was only counted if the water molecule had two pairwise interactions with the solvent molecules that were below $-4.0$ kcal mol$^{-1}$. This definition of a hydrogen bond is reasonable given the distribution in Fig. 11 and that the average energy of a hydrogen bond for classical rigid classical SPC water [116] is $-4.34$ kcal mole$^{-1}$. The resulting rate should represent an upper bound on the rate of flipping of the "special" bond and hence the rate of proton transfer. The resulting rates are plotted as a function of the oxygen–oxygen distance $R_c$ in Figure 12. As can be seen from that figure, the overall rate is significantly lower in the quantum case (which was calculated using CMD). The quantum rate in the range of $R_c = 2.5 - 2.6$ Å is in good agreement with the experimentally measured room temperature rate of the proton hop of 0.69 ps$^{-1}$ [8]. This distance range is considered to be typical of the oxygen–oxygen distances at which the "flip" of the special complex H–bond could take place. The classical rate in the same range of $R_c$ is approximately 10–20 ps$^{-1}$. The quantum rate calculation shown in Figure 12 was averaged over 20 ps of a CMD simulation, while the classical rate was

averaged over 40 ps. Clearly, the quantum effects on the nuclear motion are significant in this case.

### D. Zundel Polarization and the Continuum

Strong hydrogen bonds are characterized by low to nonexistent barriers for proton transfer, enthalpies of 9–15 kcal $mol^{-1}$, and short equilibrium distances (e.g. O–O distances less then 2.6 Å). The spectral signature of strong H–bonds in solution (and acid crystals) is a strong absorption peaked at 1500–2000 $cm^{-1}$ and extending over a range of 1000–1500 $cm^{-1}$. This absorption is known as the continuum and is observed in many liquid systems (not just water) in which symmetric H–bonds of the type $BH^+\cdots B$ or $(AH\cdots A)^-$ are present. [29] This phenomenon is a *protonic* rather than an electronic polarization effect. The polarization of a proton in a strong hydrogen has been estimated to be one to two orders of magnitude larger than electronic polarizabilities of molecules [38–40]. Two mechanisms are thought to be responsible for the continuum:

1. Zundel polarization which is also called the direct mechanism. Strong electrostatic coupling of the solvent gives rise to deformations of the proton transfer potential. There is a large distribution of fields which gives rise to a continuity of energy level differences. In addition, there is a large distribution of equilibrium H bond lengths, causing additional "smearing" of the continuum [29].

2. The indirect mechanism, which is the coupling of the OH vibration to the low frequency anharmonic O–O vibration of the proton transfer complex (or whichever two atoms are sharing the proton in a strong hydrogen bond [117–121]).

A discussion of the effects of a static external field on the absorption spectrum of the $H_5O_2^+$ complex is given by Janoschek [122]. One of the conclusions of this work and related treatises [38–40] is that the electric field produced by the surrounding polar solvent is sufficient to lead to considerable broadening of the IR absorption spectrum in strongly hy-

drogen bonded (i.e. low barrier) systems. A rigorous study to obtain the infrared absorption spectrum would require finding the line shape function $I(\omega)$ which is given by [123]

$$I(\omega) = \int_{-\infty}^{\infty} dt e^{i\omega t} \langle \mu(0)\mu(t) \rangle \quad , \tag{4.1}$$

where $\langle \mu(0)\mu(t) \rangle$ is the macroscopic quantum dipole autocorrelation function. Since only a qualitative comparison is made here, the quantum velocity autocorrelation function of the $O_1H_3$ bond is used instead, i.e.,

$$I_v(\omega) = \int_{-\infty}^{\infty} dt e^{i\omega t} \langle v_{O_1H_3}(0) v_{O_1H_3}(t) \rangle \, . \tag{4.2}$$

Since this vibrational mode is directly involved in the transfer of the proton, its power spectrum should contain most of the qualitative features of the continuum IR spectrum of a strong acid dissolved in water. Within the framework of the theory of CMD, the quantum correlation function is obtained from the centroid correlation function (which is calculated from computer simulation) using the following expression [89,90]

$$I_v(\omega) = (\hbar\beta\omega/2) \left[ \coth (\hbar\beta\omega/2) + 1 \right] I_v^{(c)}(\omega), \tag{4.3}$$

where $I_v^{(c)}(\omega)$ is the Fourier transform of the centroid velocity correlation function. The power spectrum is plotted in Figure 13 and was obtained by averaging over four ps of a CMD run. The strong absorption between 1000 and 2500 $cm^{-1}$ is typical of strong acids in solution. Some residual absorption at 3600 $cm^{-1}$ is present from the OH covalent stretch. As stated earlier the absorption is thought to occur via two mechanisms; the direct mechanism due to solvent deformations of the proton potential giving rise to a continuum of transition and the indirect mechanism due to coupling of the OH stretch to the low frequency O–O vibration. Differentiation between the two mechanisms could be made by constraining the oxygen–oxygen distance in the complex, thus eliminating the contribution of the indirect mechanism. Future work will focus on this. The spectrum presented here is also in good agreement with simulations of condensed phase proton transfer in a model system by Borgis et al. [124].

## V. CONCLUDING REMARKS

In this paper, structural and dynamical studies of an excess proton in water have been carried out. The coordination number of the $H_3O^+$ species was found to be in good agreement with experiment and the classical radial distribution functions of the $H_5O_2^+$ species are in accord with those found from *ab initio* MD methods. Importantly, the nuclear quantum effects are found to be large, accordingly the proton transfer along the strong hydrogen bond in the $H_5O_2^+$ complex is found to be a quantum activationless process. The strong hydrogen bond in the complex is considered to be a "special" bond [31] characterized by a smaller than normal oxygen–oxygen distance ($\approx 2.5$ Å) which can lead to the rapid interchange of the chemical and hydrogen bonds as the proton moves back and forth. As a result of our dynamical study of the conditions necessary for this to occur, the activation energy and rate constant measured by Luz and Meiboom [8] would seem to correspond to the flipping of the special bond to another pair of oxygens. The flipping of the special bond corresponds to the simplest example of the Grötthus mechanism of proton transfer, and it depends on the dynamics of the water molecules in the second solvation shell, of the proton transfer complex, as well as the oxygen–oxygen distance fluctuations of water molecules that hydrogen bond to the complex. Analysis of the quantum dynamics of the water molecules which hydrogen bond to the $H_5O_2^+$ complex show that the rate of inward oxygen–oxygen fluctuations of these molecules, when correlated with solvent hydrogen bonding from water molecules in the second solvation shell, is in agreement with the experimentally measured rate of proton transfer. The nuclear quantum effects in this process are significant.

Finally, the quantum power spectrum of the proton transfer mode of the $H_5O_2^+$ complex in water was found to be in qualitative agreement with the the IR spectrum of strong hydrogen bonding systems, showing a characteristic broad absorption. Future work will be devoted to exploration of whether the direct or indirect mechanism predominates in the calculated spectrum, as well as to actual quantum simulations of the extended proton migration process.

## VI. ACKNOWLEDGMENTS

This research was supported by the National Science Foundation (CHE–9158079 and CHE–9410608) and by the Office of Naval Research. The computations in this study were supported in part by a grant of computer time from the National Science Foundation Supercomputer Centers under grant number MCA94P017. Some of the computations were also carried out on an IBM SP2 parallel computer purchased in part through an NSF Academic Research Infrastructure grant (DMR94–13373). GAV is a recipient of a National Science Foundation Presidential Young Investigator Award, a David and Lucile Packard Fellowship in Science and Engineering, an Alfred P. Sloan Foundation Research Fellowship, and a Camille Dreyfus Teacher–Scholar Award. The authors are indebted to Jianshu Cao and Diane Sagnella for valuable advice and to Marc Pavese and Amir Karger for proofreading the manuscript. The authors would also like to acknowledge Kari Laasonen and Mark Tuckerman for helpful discussions.

# REFERENCES


[1] P. W. Atkins, *Physical Chemistry*, 5th ed. (W. H. Freeman, New York, 1994).

[2] J. D. Bernal and R. H. Fowler, J. Chem. Phys. **1**, 515 (1933).

[3] B. E. Conway, J. O. Bockris, and H. Linton, J. Chem. Phys. **24**, 834 (1956).

[4] J. O. Bockris and A. K. N. Reddy, *Modern Electrochemistry* (Plenum Press, New York, 1970), Vol. 1, Chap. 5.

[5] T. Komatsuzaki and I. Ohmine, Chem. Phys. **180**, 239 (1994).

[6] M. D. Newton and S. Eherenson, J. Am. Chem. Soc. **93**, 4971 (1971).

[7] M. D. Newton, J. Chem. Phys. **67**, 5535 (1977).

[8] Z. Luz and S. Meiboom, J. Am. Chem. Soc. **86**, 4768 (1964).

[9] B. Halle and G. Karlström, J. Chem. Faraday Trans. 2 **79**, 1047 (1983).

[10] *The Physics and Chemistry of Ice*, edited by E. Whalle, S. J. Jones, and L. W. Gold (Royal Society of Canada, Ottawa, 1973).

[11] M. Eigen and L. D. Maeyer, Proc. Roy. Soc. A **247**, 505 (1958).

[12] M. Eigen, Angnew. Chem. (Int. edn) **3**, 1 (1964).

[13] D. Eisenberg and W. Kauzman, *The Structure and Properties of Water* (Oxford University Press, Oxford, 1969).

[14] Y. Xie, R. B. Remington, and H. F. Schaefer III, J. Chem. Phys. **101**, 4878 (1994).

[15] C. Mijoule, Z. Latajka, and D. Borgis, Chem. Phys. Lett. **208**, 364 (1993).

[16] K. Luth and S. Scheiner, J. Chem. Phys. **97**, 7507 (1992).

[17] S. Scheiner, Acc. Chem. Res. **18**, 174 (1985).

[18] S. Scheiner, J. Am. Chem. Soc. **103**, 315 (1981).

[19] Z. Latajka and S. Scheiner, J. Mol. Struc. (Theochem) **234**, 373 (1991).

[20] S. Scheiner, J. Phys. Chem. **86**, 376 (1982).

[21] R. P. Bell, *The Proton in Chemistry*, 2nd ed. (Cornell University Press, Ithaca, NY, 1973).

[22] R. P. Bell, *The Tunnel Effect in Chemistry* (Chapman and Hall, London, 1980).

[23] D. J. Barnest and R. P. Bell, Proc. R. Soc. London A. **318**, 421 (1970).

[24] *Proton Transfer Reactions*, edited by E. F. Caldin and V. Gold (Chapman and Hall, London, 1975).

[25] E. F. Caldin, Chem. Rev. **69**, 135 (1969).

[26] B. Halle and G. Karlström, J. Chem. Faraday Trans. 2 **79**, 1031 (1983).

[27] P. A. Giguère and S. Turrell, Can. J. Chem. **54**, 3477 (1976).

[28] R. Triolo and A. H. Narten, J. Chem. Phys. **63**, 3624 (1975).

[29] G. Zundel, in *The Hydrogen Bond: Recent Developments in Theory and Experiment*, edited by P. Schuster, G. Zundel, and C. Sandory (North-Holland, Amsterdam, 1976), Vol. 2, Chap. 15.

[30] T. Ackermann, Z. Phys. Chem. **27**, 253 (1961).

[31] M. Tuckerman, K. Laasonen, M. Sprik, and M. Parrinello, J. Phys. Chem. **99**, 5749 (1995).

[32] The notation $H_9O_4^+$ implies that the hydronium is symmetrical with three equivalent hydrogens and three hydrogen–bonded water molecules. The notation $H_5O_2^+$ denotes that the transferring proton is equally shared between the hydronium and one of the accompanying water molecules in the first solvation shell, creating a strongly hydrogen–bound complex.

[33] G. Karlström, J. Phys. Chem. **92**, 1315 (1988).

[34] G. Karlström, J. Phys. Chem. **92**, 1318 (1988).

[35] I. Tuñón, E. Silla, and J. Bertrán, J. Phys. Chem. **97**, 5547 (1993).

[36] F. R. Tortonda, J. Pascual-Ahuir, E. Silla, and I. Tuñón, J. Phys. Chem. **97**, 11087 (1993).

[37] K. Laasonen and M. L. Klein, J. Phys. Chem. **98**, 10079 (1994).

[38] R. Jansochek, E. G. Weidman, H. Pfeiffer, and G. Zundel, J. Am. Chem. Soc. **94**, 2387 (1972).

[39] R. Janoschek, in *The Hydrogen Bond: Recent Developments in Theory and Experiment*, edited by P. Schuster, G. Zundel, and C. Sandorfy (North Holland, Amsterdam, 1976), Vol. 1, Chap. 3.

[40] See also Ref. [29].

[41] K. Ando and J. T. Hynes, preprint (1995).

[42] S. L. Fornili, M. Migliore, and M. A. Palazzo, Chem. Phys. Lett. **125**, 419 (1986).

[43] R. E. Kozack and P. C. Jordan, J. Chem. Phys. **96**, 3131 (1992).

[44] R. E. Kozack and P. C. Jordan, J. Chem. Phys. **96**, 3120 (1992).

[45] K. Laasonen, M. Sprik, M. Parrinello, and R. Car, J. Phys. Chem. **99**, 9080 (1995).

[46] M. Tuckerman, K. Laasonen, M. Sprik, and M. Parrinello, J. Phys. Chem. **99**, 5749 (1995).

[47] M. Tuckerman, K. Laasonen, M. Sprik, and M. Parrinello, J. Phys. C. **6**, 93 (1994).

[48] K. Laasonen and M. L. Klein, J. Am. Chem. Soc. **116**, 11620 (1994).

[49] R. Car and M. Parrinello, Phys. Rev. Lett. **55**, 2471 (1985).

[50] C. Galli and M. Parrinello, in *Computer Simulations in Material Science*, edited by M. Meyer and V. Pontikis (Kluwer, Dordrecht, 1991), p. 283.

[51] R. Car and M. Parrinello, in *Simple Molecular Systems at Very High Density*, edited by A. Poliani, P. Louberyre, and N. Boccara (Plenum, New York, 1989), p. 455.

[52] D. K. Remler and P. A. Madden, Mol. Phys. **70**, 921 (1990).

[53] A. Warshel and R. M. Weiss, J. Am. Chem. Soc. **102**, 6218 (1980).

[54] A. Warshel, *Computer Modeling of Chemical Reactions in Enzymes and Solutions* (J. Wiley and Sons, New York, 1991).

[55] D. Laria, G. Ciccotti, M. Ferrario, and R. Kapral, J. Chem. Phys. **97**, 378 (1992).

[56] J. Lobaugh and G. A. Voth, Chem. Phys. Lett. **198**, 311 (1992).

[57] H. Azzouz and D. Borgis, J. Chem. Phys. **98**, 7361 (1993).

[58] J. Lobaugh and G. A. Voth, J. Chem. Phys. **100**, 3039 (1994).

[59] G. A. Voth, D. Chandler, and W. H. Miller, J. Chem. Phys. **91**, 7749 (1989).

[60] G. A. Voth, Chem. Phys. Lett. **170**, 289 (1990).

[61] G. A. Voth, J. Phys. Chem. **97**, 8365 (1993), and references cited therein.

[62] M. J. Gillan, J. Phys. C **20**, 3621 (1987).

[63] D. H. Li and G. A. Voth, J. Phys. Chem. **95**, 10425 (1991).

[64] R. P. Feynman, *Statistical Mechanics* (Addison-Wesley, Reading, MA, 1972).

[65] B. J. Berne and D. Thirumalai, Annu. Rev. Phys. Chem. **37**, 401 (1987).

[66] D. L. Freeman and J. D. Doll, Adv. Chem. Phys. **70B**, 139 (1988).

[67] J. D. Doll and D. L. Freeman, Adv. Chem. Phys. **73**, 289 (1989).

[68] *Quantum Simulations of Condensed Matter Phenomena*, edited by J. D. Doll and J. E. Gubernatis (World Scientific, Singapore, 1990).

[69] D. Chandler, in *Liquides, Cristallisation et Transition Vitreuse, Les Houches, Session LI*, edited by D. Levesque, J. P. Hansen, and J. Zinn-Justin (Elsevier Science Publishers B.V., Amsterdam, 1991).

[70] M. Parrinello and A. Rahman, J. Chem. Phys. **80**, 860 (1984).

[71] J. P. Valleau and G. M. Torrie, in *Statistical Mechanics, part A*, edited by B. J. Berne (Plenum Press, New York, 1977).

[72] D. Chandler and P. G. Wolynes, J. Chem. Phys. **74**, 4078 (1981).

[73] K. S. Schweizer, R. M. Stratt, D. Chandler, and P. G. Wolynes, J. Chem. Phys. **75**, 1347 (1981).

[74] E. J. Heller and S. Tomsovic, Physics Today 38 (1993).

[75] E. J. Heller, Acct. Chem. Research **14**, 368 (1981).

[76] E. J. Heller, J. Chem. Phys. **75**, 2923 (1981).

[77] S. Tomsovic and E. J. Heller, Phys. Rev. Lett. **67**, 664 (1991).

[78] E. J. Heller, J. Chem. Phys. **94**, 2723 (1991).

[79] W. H. Miller, Adv. Chem. Phys. **25**, 69 (1974).

[80] W. H. Miller, Science **233**, 171 (1986).

[81] D. F. Coker, in *Computer Simulation in Chemical Physics*, edited by M. P. Allen and D. J. Tildesley (Kluwer Academic Publishers, Holland, 1993), p. 315.

[82] J. C. Tully, J. Chem. Phys. **93**, 1061 (1990).

[83] For applications of this method to proton transfer, see Ref. [84,85].

[84] S. Hammes-Schiffer and J. C. Tully, J. Chem. Phys. **101**, 4657 (1994).

[85] S. Hammes-Schiffer and J. C. Tully, J. Phys. Chem. **95**, 5793 (1995).

[86] F. J. Webster, P. J. Rossky, and R. A. Friesner, Comput. Phys. Commun. **63**, 494 (1991).

[87] F. J. Webster, J. Schnitker, M. S. Friedrichs, R. A. Friesner and P. J. Rossky, Phys. Rev. Lett. **66**, 3172 (1991).

[88] J. Cao and G. A. Voth, J. Chem. Phys. **99**, 10070 (1993).

[89] J. Cao and G. A. Voth, J. Chem. Phys. **100**, 5106 (1994).

[90] J. Cao and G. A. Voth, J. Chem. Phys. **101**, 6157 (1994).

[91] J. Cao and G. A. Voth, J. Chem. Phys. **101**, 6168 (1994).

[92] For notational simplicity, we refer to $\mathbf{R}_{\mathrm{H}}^{(i)}$ as a general $(3N_{\mathrm{H}}+3)$–dimensional vector of the coordinates of the protons $\left\{\mathbf{R}_{\mathrm{H}_1}^{(i)},...,\mathbf{R}_{\mathrm{H}_{N_{\mathrm{H}}}}^{(i)};\mathbf{r}^{(i)}\right\}$ and $\mathbf{R}_{\mathrm{O}}$ as a general $3N_{\mathrm{O}}$–dimensional vector of the coordinates of the oxygens $\left\{\mathbf{R}_{\mathrm{O}_1},...,\mathbf{R}_{\mathrm{O}_{N_{\mathrm{O}}}}\right\}$.

[93] R. Giachetti and V. Tognetti, Phys. Rev. Lett. **55**, 912 (1985).

[94] R. Giachetti and V. Tognetti, Phys. Rev. B **33**, 7647 (1986).

[95] R. P. Feynman and H. Kleinert, Phys. Rev. A. **34**, 5080 (1986).

[96] J. Cao and G. A. Voth, J. Chem. Phys. **100**, 5093 (1994).

[97] R. Hernandez, J. Cao, and G. A. Voth, J. Chem. Phys. **102**, xxxx (1995).

[98] M. Pavese and G. A. Voth, , (manuscript in preparation).

[99] L. I. Yeh, M. Okumura, J. D. Myers, J. M. Price and Y. T. Lee, J. Chem. Phys. **91**, 7319 (1989).

[100] K. Kutchitsu and Y. Morino, Bull. Chem. Soc. Jpn. **38**, 814 (1965).

[101] K. Toukan and A. Rahman, Phys. Rev. B **31**, 2643 (1985).

[102] D. Wei and D. R. Salahub, J. Chem. Phys. **101**, 7633 (1994).

[103] H. J. C. Berendson, J. P. M. Postma, W. F. van Gunsteren, and J. Hermans, in *Intermolecular Forces*, edited by B. Pullman (Reidel, Dordrecht, 1981).

[104] J. Lobaugh, M. Pavese, and G. A. Voth, , (manuscript in preparation).

[105] J. B. Straus, A. Calhoun, and G. A. Voth, J. Chem. Phys. **102**, 529 (1995).

[106] R. A. Kuharski and P. J. Rossky, J. Chem. Phys. **82**, 5164 (1985).

[107] M. P. Allen and D. J. Tildesley, *Computer Simulation of Liquids* (Clarendon Press, Oxford, 1987).

[108] M. E. Tuckerman, B. J. Berne, G. J. Martyna, and M. L. Klein, J. Chem. Phys. **99**, 2796 (1993).

[109] W. C. Swope, H. C. Anderson, P. H. Berens, and K. R. Wilson, J. Chem. Phys. **76**, 637 (1982).

[110] S. Nosé, Mol. Phys. **52**, 255 (1984).

[111] S. Nosé, J. Chem. Phys. **81**, 511 (1984).

[112] W. G. Hoover, Phys. Rev. A **31**, 1695 (1985).

[113] R. W. Hall and B. J. Berne, J. Chem. Phys. **81**, 3641 (1984).

[114] G. J. Martyna, M. L. Klein, and M. Tuckerman, J. Chem. Phys. **97**, 2635 (1992).

[115] The constraint force on each quasiparticle can easily be shown to be -$\mathbf{F}_{\mathrm{H}}^{(c)}/P$ with the method of Lagrange multipliers .

[116] W. L. Jorgenson, J. Chandrasekhar, J. D. Madura, R. W. Impey, and M. L. Klein, J. Chem. Phys. **79**, 926 (1983).

[117] S. Bratos, J. Chem. Phys. **63**, 3499 (1975).

[118] S. Bratos and H. Ratajczak, J. Chem. Phys. **76**, 77 (1982).

[119] G. N. Robertson and J. Yardwood, Chem. Phys. **32**, 267 (1978).

[120] V. P. Sakun, Chem. Phys. **55**, 27 (1981).

[121] V. P. Sakun, Chem. Phys. **76**, 77 (1982).

[122] R. Janoschek, E. G. Weidemann, and G. Zundel, J. Chem. Faraday Trans. 2 **69**, 505 (1973).

[123] G. C. Schatz and M. A. Ratner, *Quantum Mechanics in Chemistry* (Prentice Hall, Englewood Cliffs, New Jersey, 1993).

[124] D. Borgis, G. Tarjus, and H. Azzouz, J. Chem. Phys. **97**, 1390 (1992).

[125] Calculated by a normal mode analysis of $V_{intra}^{H_3O^+}$.

## TABLES

TABLE I. Experimental [27,99] and model [125] vibrational frequencies of the hydronium ion in $cm^{-1}$.

| | | | | |
|---|---|---|---|---|
| Expt. | 1200 | 1700 | 3645 | 3730 |
| Model | 1101 | 1704 | 3610 | 3725 |

TABLE II. Intramolecular water and hydronium parameters.

| Parameter | Value |
|---|---|
| $k_{OH}$ | 546 kcal mol$^{-1}$ Å$^{-2}$ |
| $r_0$ | 0.98 Å |
| $k_\theta$ | 44.55 kcal mol$^{-1}$ radian$^{-2}$ |
| $\theta_0$ | 110 degrees |
| $\rho_w$ | 2.566 Å |
| $D_w$ | 0.708 mdyn Å |
| $b_{OH_{eq}}$ | 1.0 Å |
| HOH angle | 109.47 degrees |
| $b$ | 2.283 mdyn Å$^{-1}$ |
| $c$ | -1.469 mdyn Å$^{-1}$ |
| $d$ | 0.776 mdyn Å$^{-1}$ |

TABLE III. Intermolecular potential parameters for the hydronium and water.

| O–O | | $H_2O$ | | $H_3O^+$ | |
|---|---|---|---|---|---|
| $\epsilon/k_B$ (K) | $\sigma$ (Å) | $q_O$ (e) | $q_H$ (e) | $q_O$ (e) | $q_H$ (e) |
| 78.22 | 3.165 | -0.83826 | 0.45212 | -0.641 | 0.52518 |

TABLE IV. Charge switching parameters used in Eq. (3.12)–(3.16).

| Parameter | Value |
|---|---|
| $e_{\mathrm{O}}^{\mathrm{H_3O^+}}$ | -0.64151 e |
| $e_{\mathrm{O}}^{\mathrm{H_2O}}$ | -0.83826 e |
| $e_{\mathrm{H}}^{\mathrm{H_3O^+}}$ | 0.52804 e |
| $e_{\mathrm{H}}^{\mathrm{H_2O}}$ | 0.45212 e |
| $e_{\mathrm{H}t}$ | 0.51945 e |
| $q_{min}^{H}$ | 0.58575 e |
| $\alpha_{sw}$ | 10.8396 $\mathrm{Å}^{-4}$ e |
| $q_{sw}$ | 0.3175 Å |

## FIGURES

FIG. 1. Illustration of the Grötthus mechanism. Charge transfer takes place via an interchange of chemical and hydrogen bonds.

FIG. 2. Schematic of the proton transfer reaction coordinate and atoms of the proton transfer complex. The transferring proton is labeled $H_3$ and $r_1$ ($r_2$) is the distance between $H_3$ and $O_1$ ($O_2$). Also illustrated are four water molecules adjacent to the complex and the critical second O–O ($R_c$) distance (cf. Sec. IV C).

FIG. 3. Diabatic states of the $H_5O_2^+$ complex.

FIG. 4. Gas phase empirical potential energy surface of the $H_5O_2^+$ complex as a function of the $O_1$–$O_2$ distance and $O_1$–$H_3$ distance. The contours are in 1.0 kcal $mol^{-1}$ increments.

FIG. 5. Plot of the *ab initio* gas phase charges of atoms of the $H_5O_2^+$ complex and empirical charge switching functions used to reproduce the *ab initio* results. Charges are plotted as a function of the proton transfer reaction coordinate. The charge on $H_2$ is the same as $H_1$. Charges on $H_4$ and $H_5$ are the mirror image of $H_1$, reflected about $q_{asym} = 0$. Similarly, the charge on $O_2$ is the mirror image of $O_1$.

FIG. 6. Radial distributions of oxygen atoms of the $H_5O_2^+$ complex with respect to the solvent and complex oxygen atoms. Radial distributions are shown for the quantum (solid) and classical (dashed line) cases. The classical oxygen–oxygen distribution function (dot-dashed) of SPC/F water is also shown for comparison.

FIG. 7. Radial distribution of water hydrogens as well as the transferring proton with respect to the oxygen atoms of the complex (quantum-solid, classical-dashed). The classical SPC/F oxygen–hydrogen distribution function of liquid water is also shown for comparison.

FIG. 8. Radial distribution of water hydrogens and covalently bound complex hydrogens with respect to the transferring proton of the complex. The quantum distribution is the solid line while the classical the dashed line. The classical hydrogen–hydrogen distribution function of liquid water (SPC/F) is also shown for comparison.

FIG. 9. Trajectory of the transferring proton along the asymmetric stretch coordinate in the (9a) classical and (9b) quantum centroid cases.

FIG. 10. Activation free energy curves as a function of the proton asymmetric stretch coordinate. The classical activation energy curve is shown in 10a, while the quantum activation energy curve is shown in 10b. Both free energy curves have been calculated with system sizes of 510 and 123 water molecules.

FIG. 11. Pair energy distribution of the four molecules closest to the $H_5O_2^+$ complex. The dashed line is for the classical system and the solid line is for the quantum system.

FIG. 12. The rate of oxygen–oxygen fluctuations correlated simultaneously with the hydrogen bonding of a water molecule adjacent to the complex (cf Sec. IV C). The quantum rate is shown by the solid line, while the classical rate is given by the dash-dot line.

FIG. 13. Power spectrum of the quantum velocity auto correlation function of the $O_1H_3$ bond (solid line). The broad absorption from 1000 $cm^{-1}$ to 2500 $cm^{-1}$ is typical of strong aqueous acids. Shown also is the power spectrum of one of the covalent OH bonds of the $H_5O_2^+$ complex that does not participate in the proton transfer (dashed line).

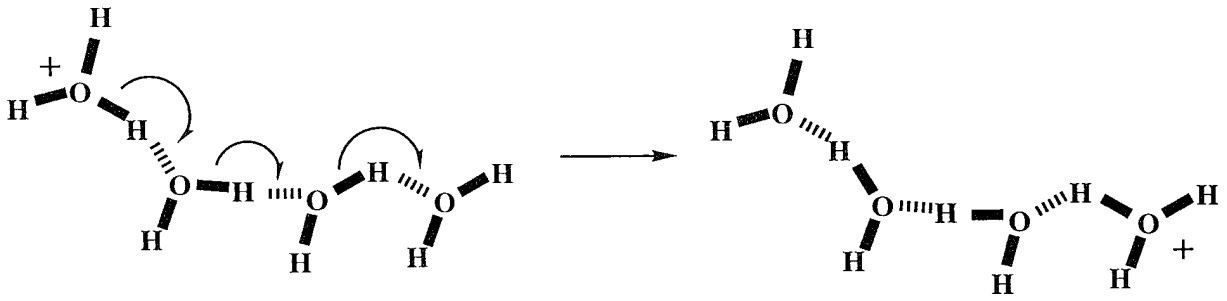

Figure 1

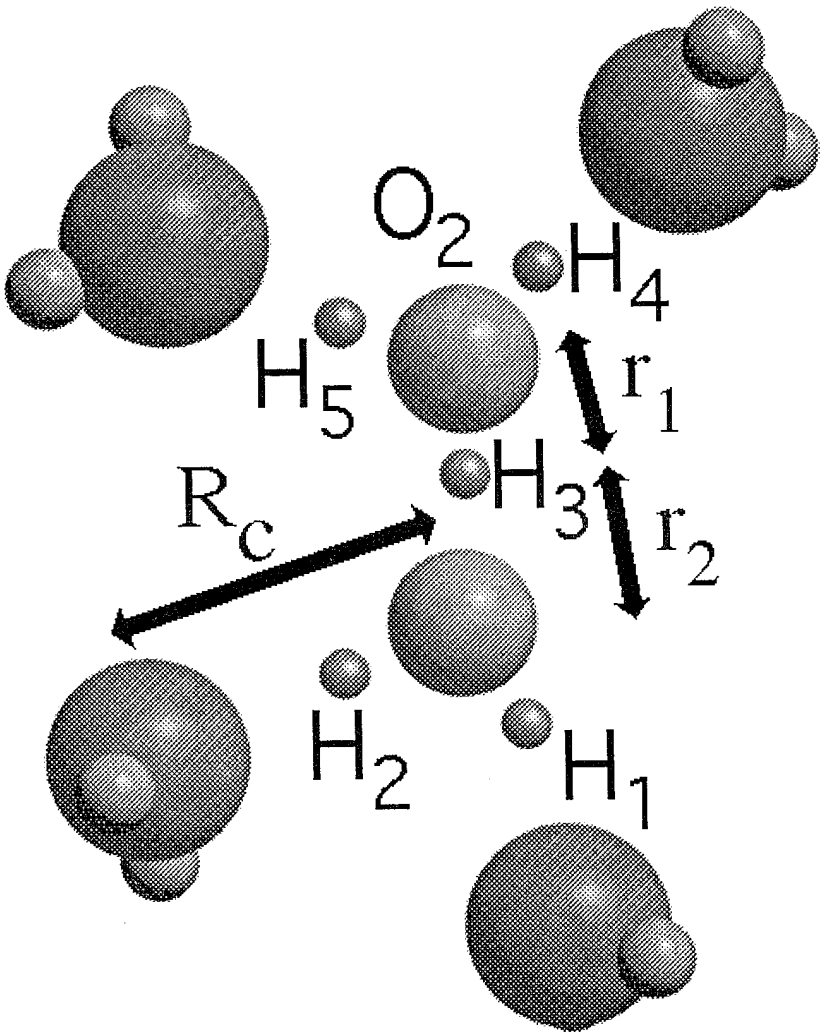


**Figure 2**

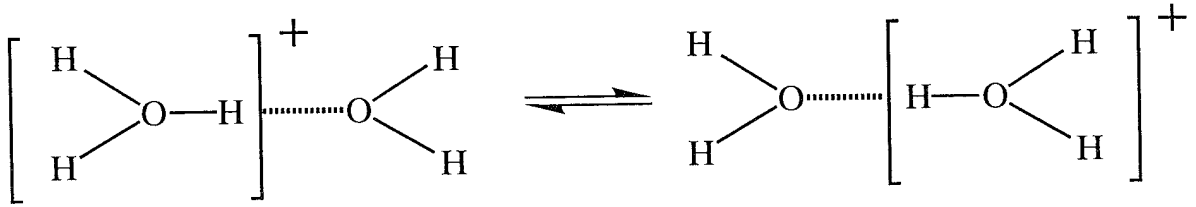

$V_{11}$ $V_{22}$

Figure 3

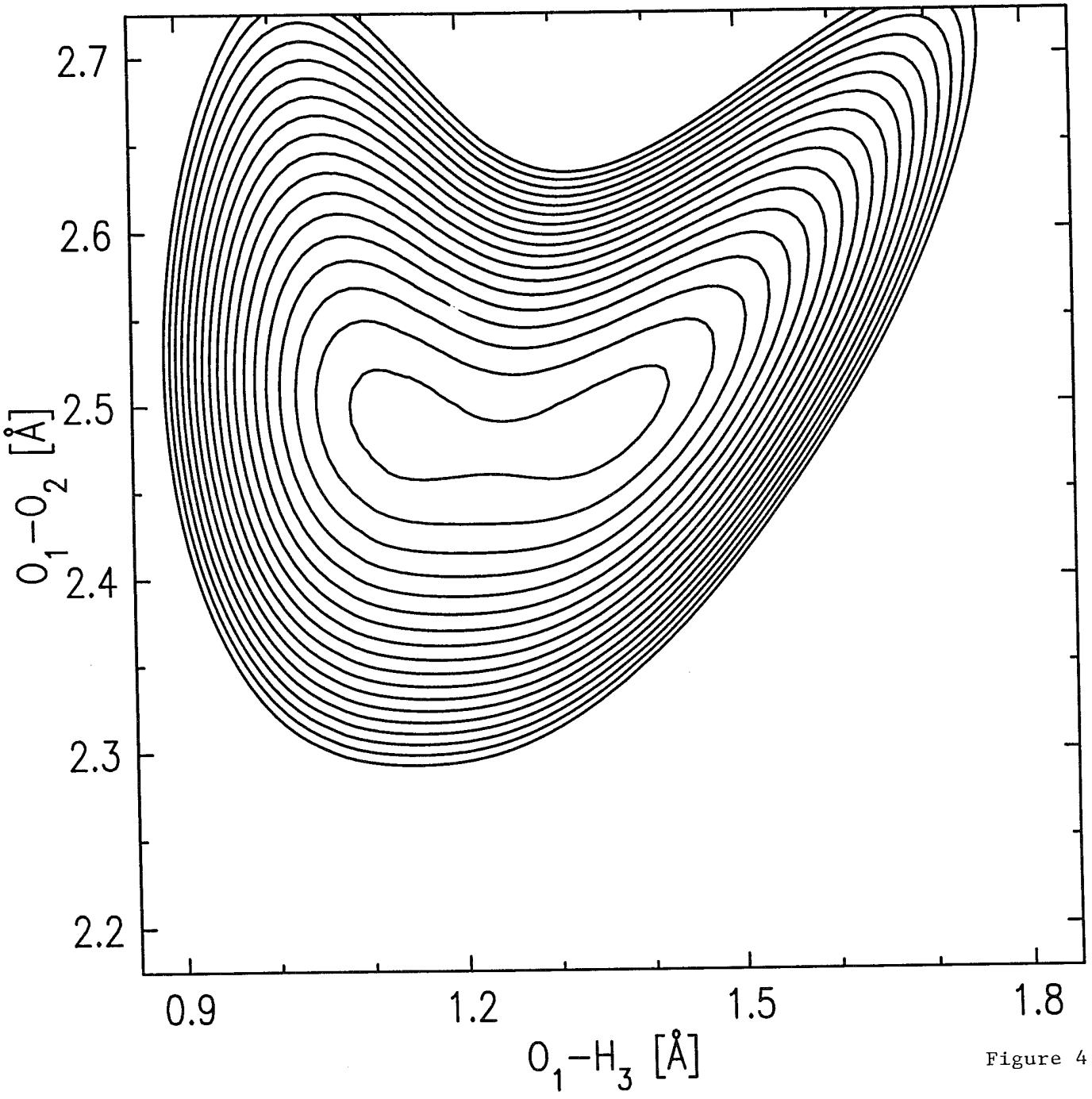


Figure 4

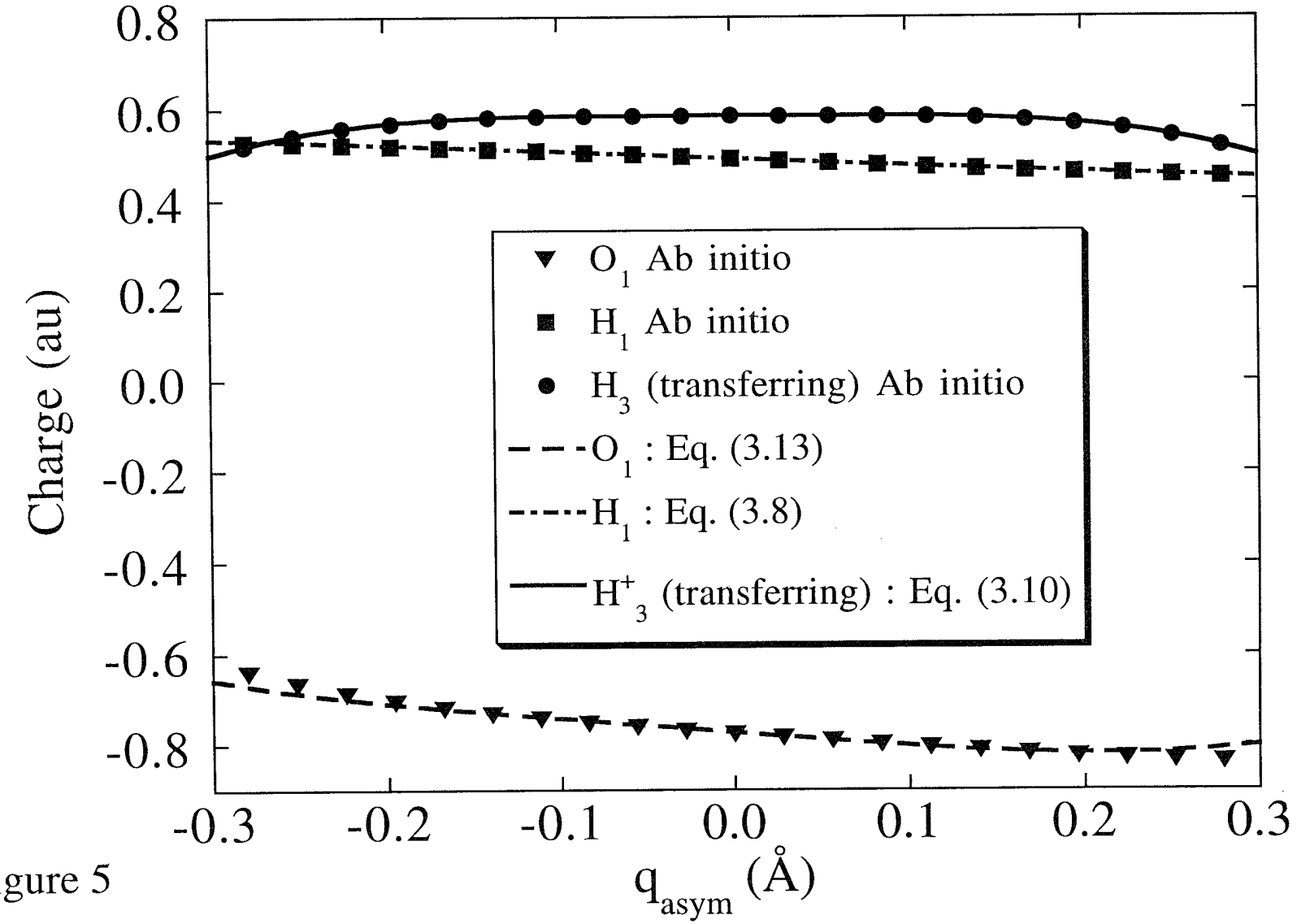
0.8
0.6
0.4
0.2
0.0
-0.2
-0.4
-0.6
-0.8
Charge (au)
-0.3
-0.2
-0.1
0.0
0.1
0.2
0.3
$q_{asym}$ (Å)
$O_1$ Ab initio
$H_1$ Ab initio
$H_3$ (transferring) Ab initio
$O_1$ : Eq. (3.13)
$H_1$ : Eq. (3.8)
$H^+_3$ (transferring) : Eq. (3.10)

Figure 5

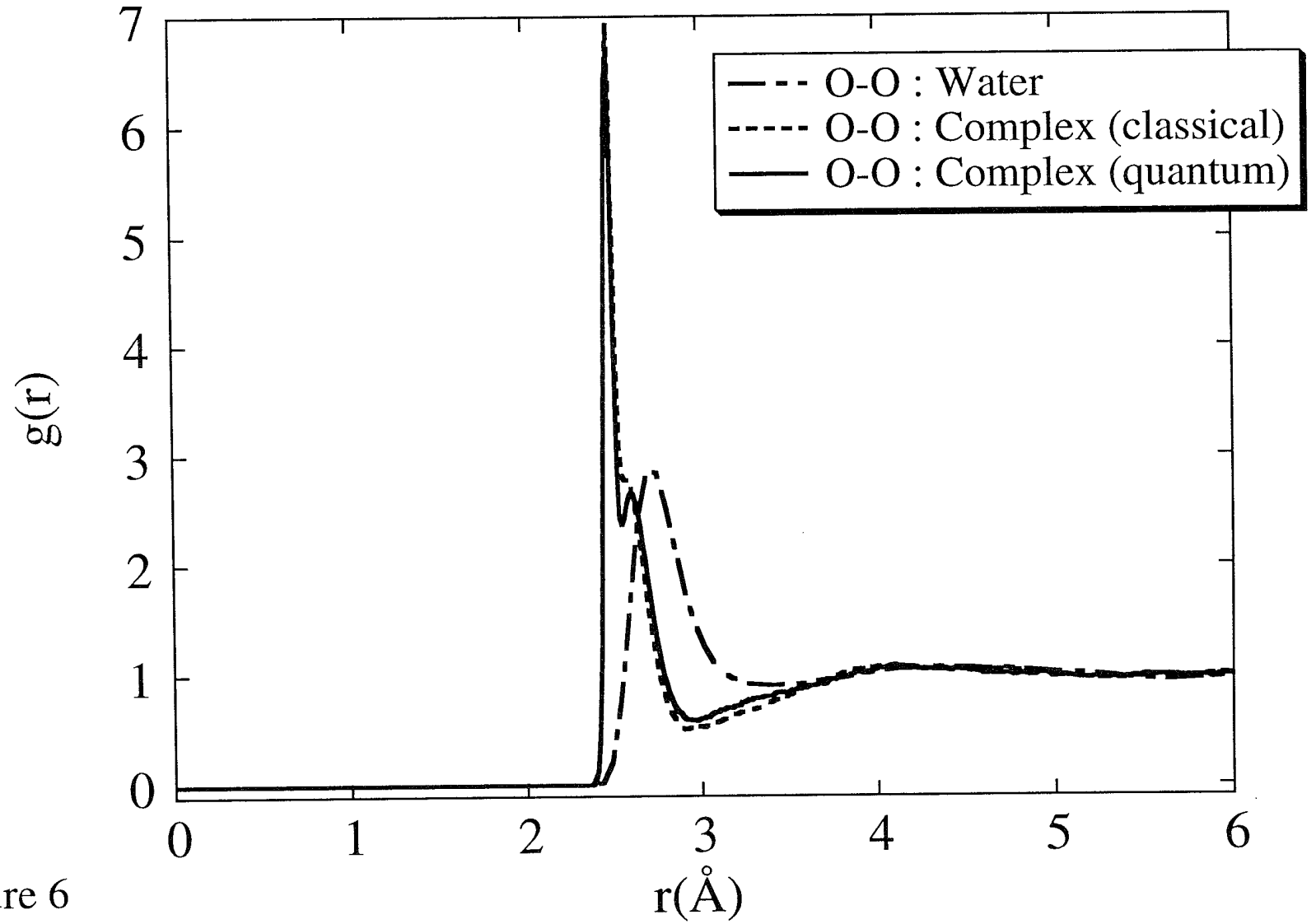
O-O : Water
O-O : Complex (classical)
O-O : Complex (quantum)
g(r)
r(Å)
0
1
2
3
4
5
6
7

Figure 6

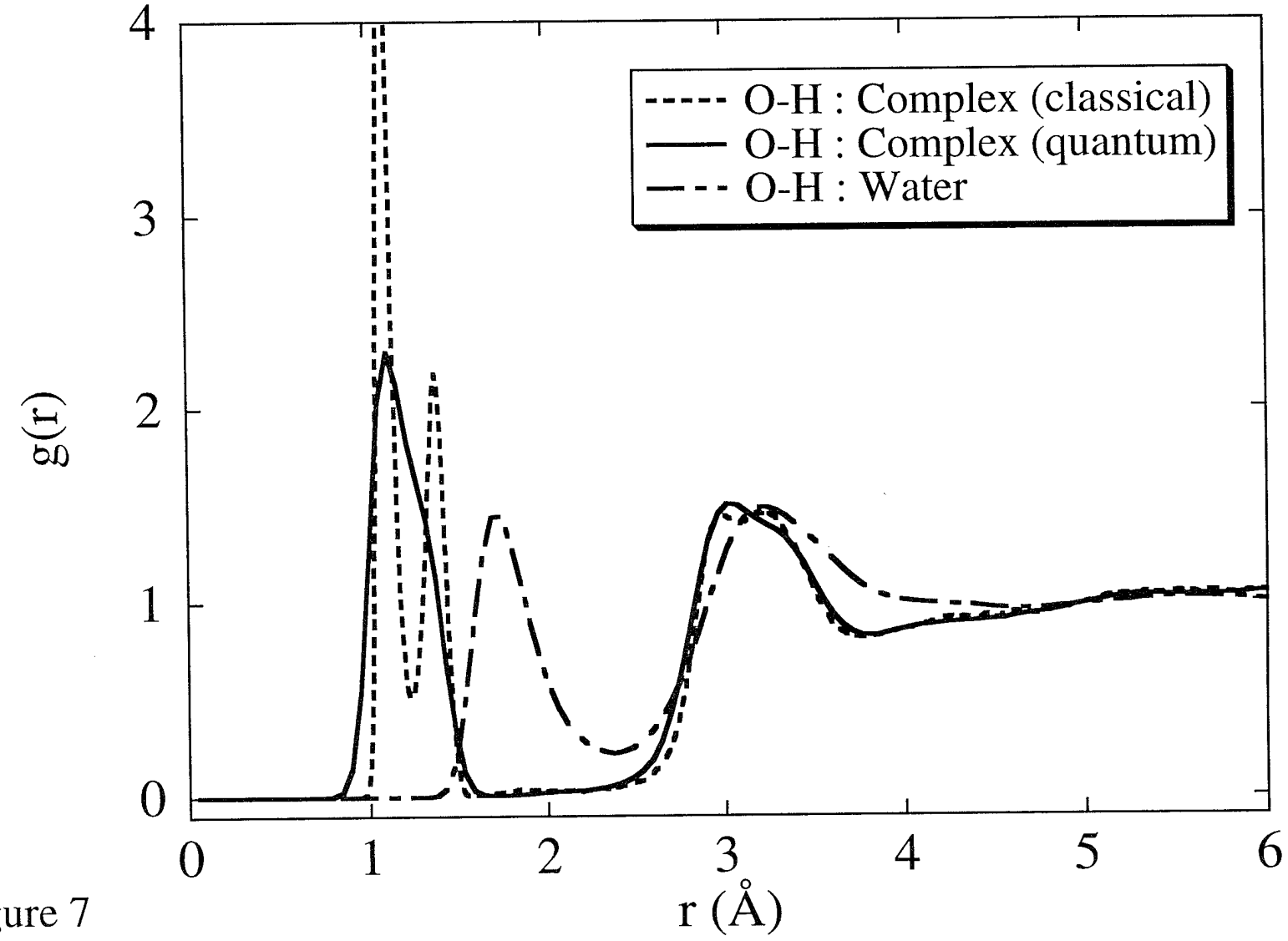
O-H : Complex (classical)
O-H : Complex (quantum)
O-H : Water
g(r)
r (Å)
0
1
2
3
4
5
6

Figure 7

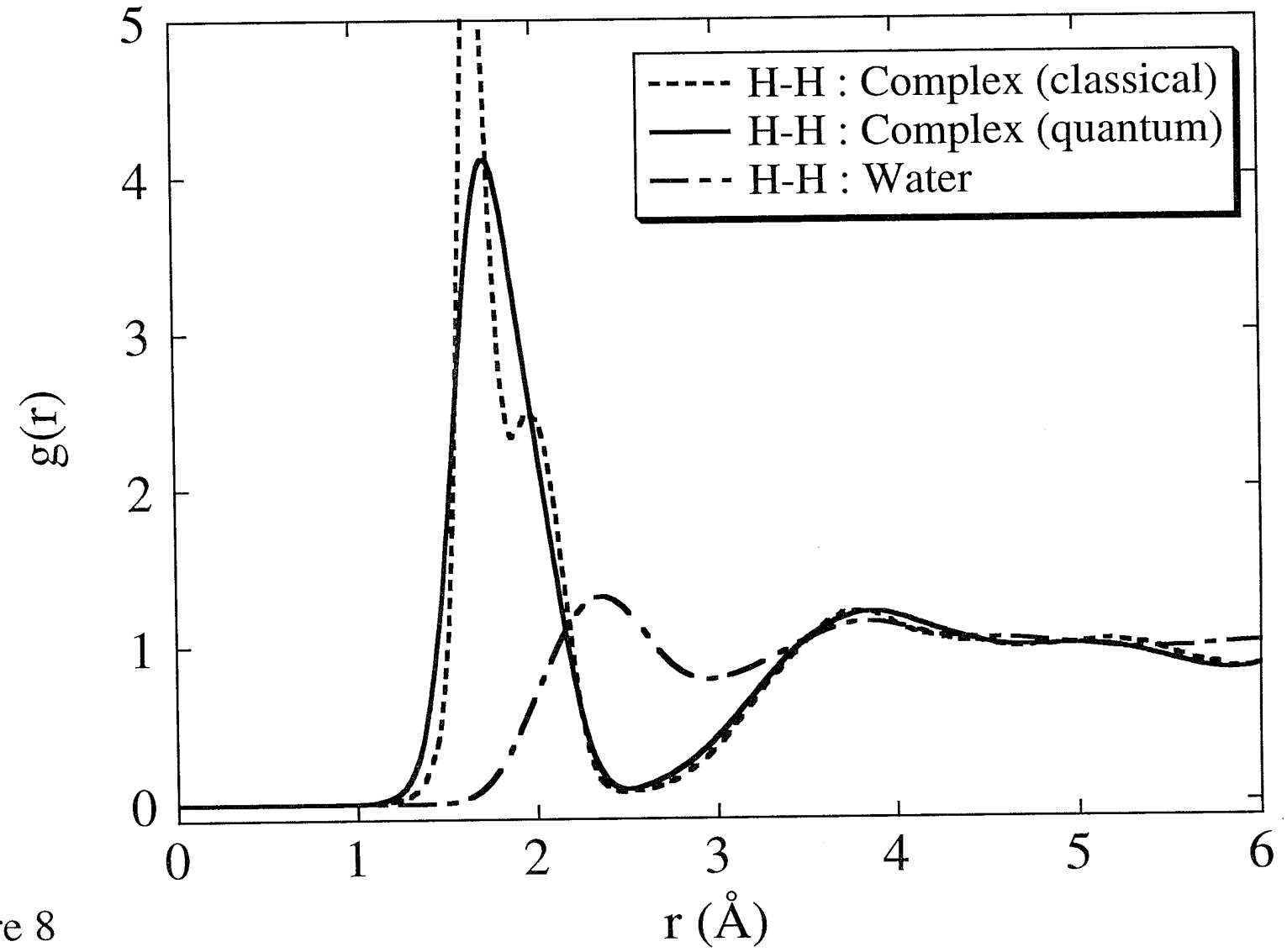
H-H : Complex (classical)
H-H : Complex (quantum)
H-H : Water
g(r)
r (Å)
0
1
2
3
4
5
6

Figure 8

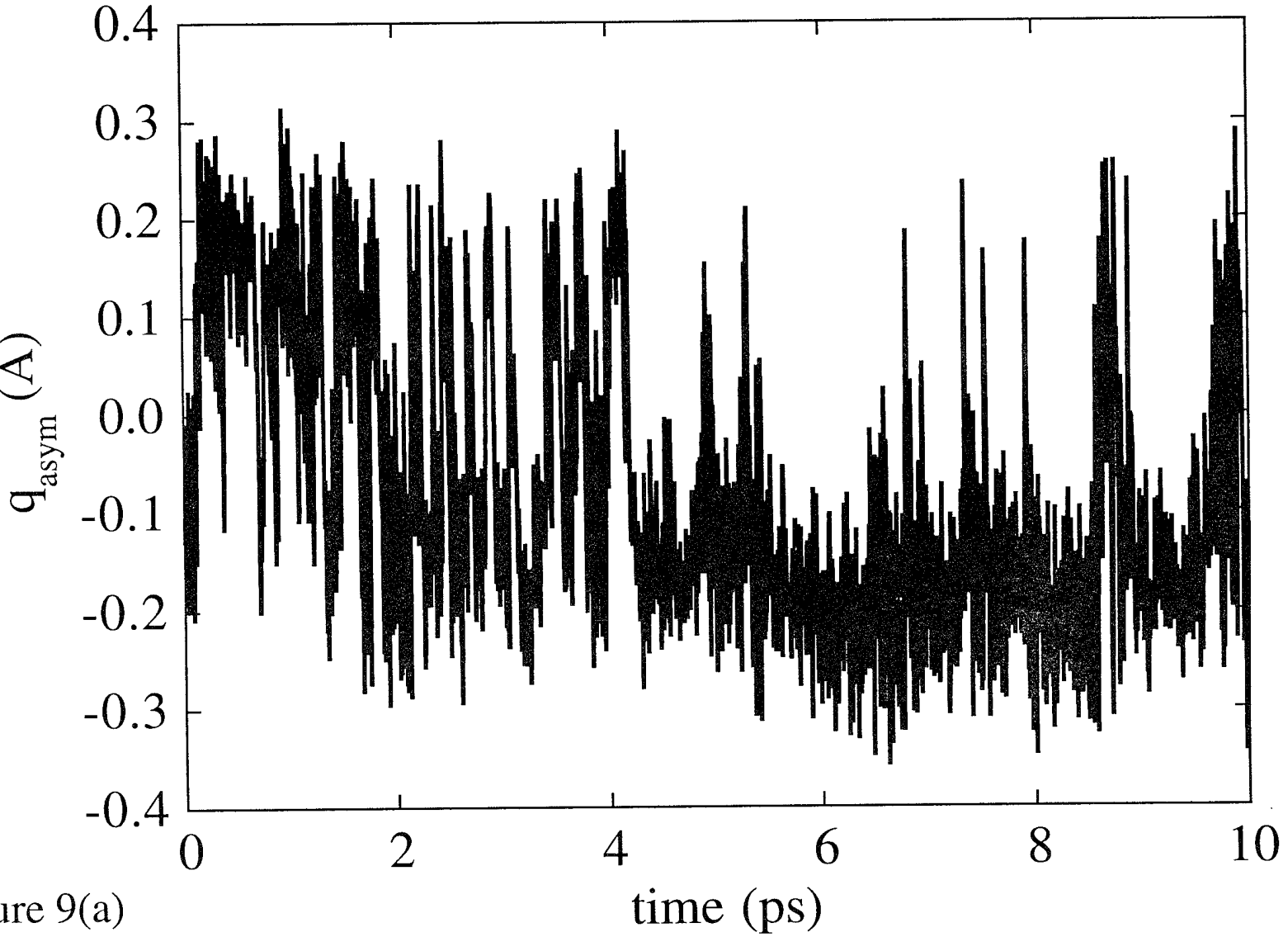


Figure 9(a)

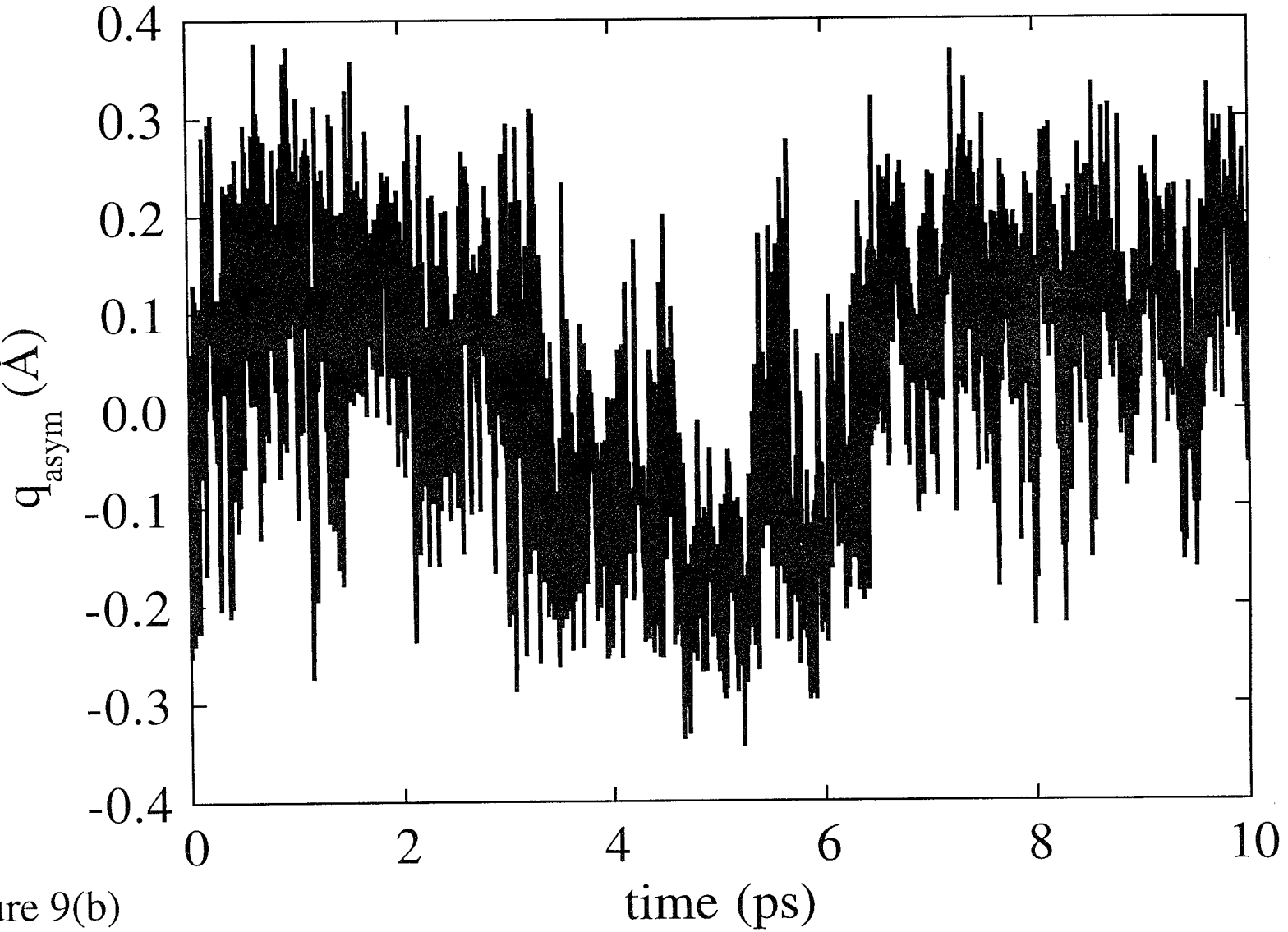


Figure 9(b)

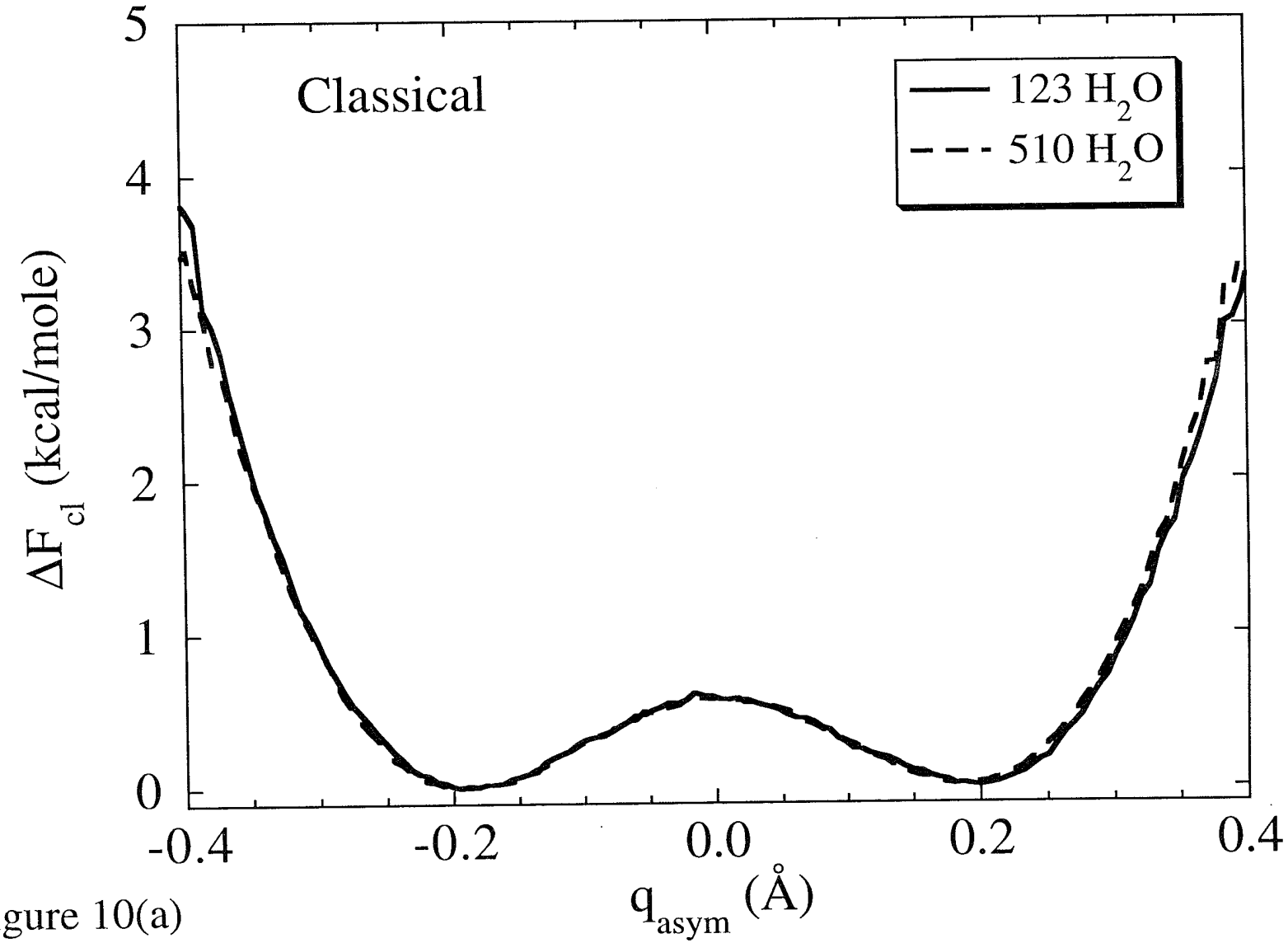
Classical
123 H2O
510 H2O
ΔFcl (kcal/mole)
qasym (Å)
5
4
3
2
1
0
-0.4
-0.2
0.0
0.2
0.4

Figure 10(a)

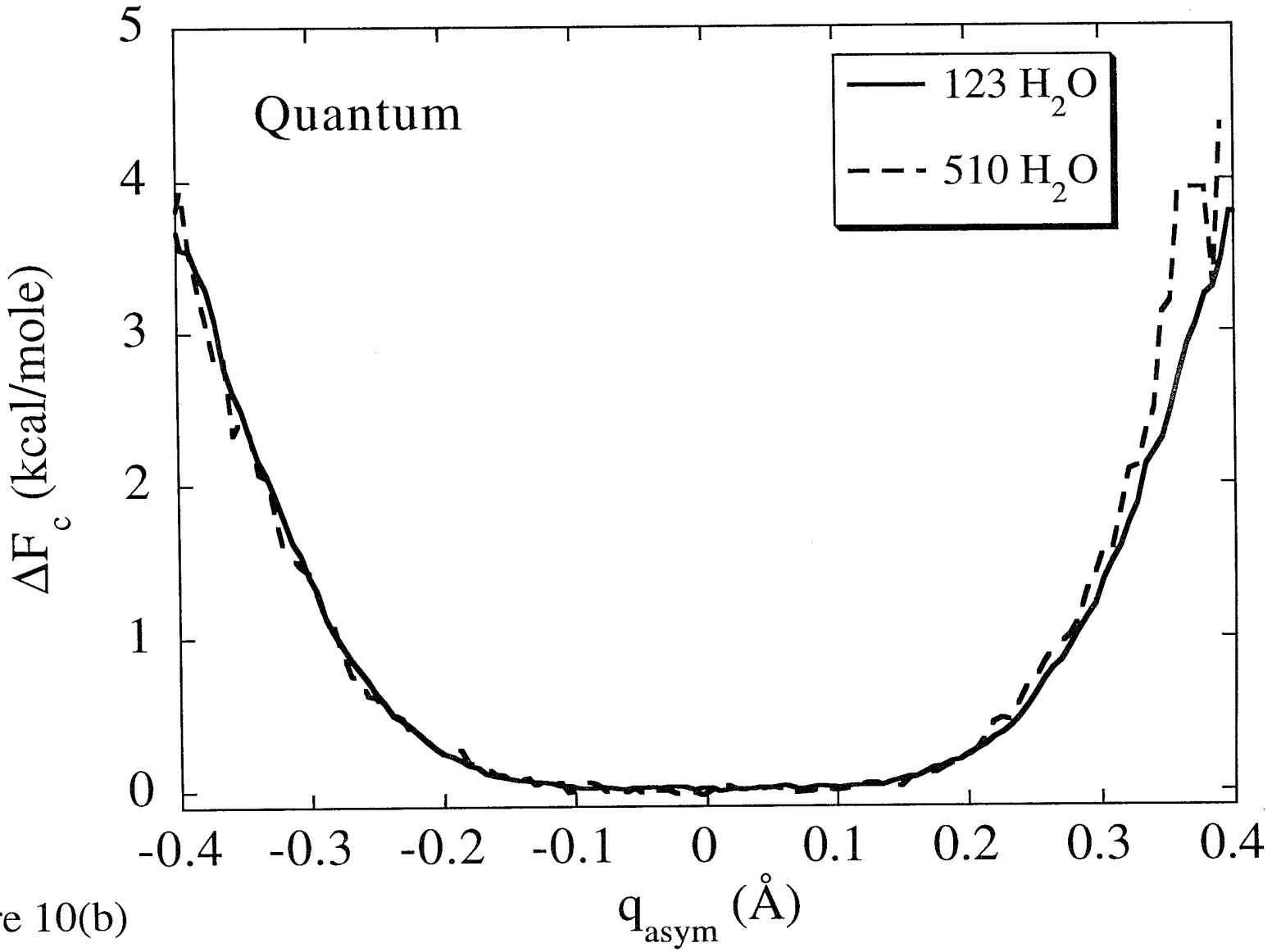
Quantum
123 H2O
510 H2O
ΔFc (kcal/mole)
qasym (Å)
5
4
3
2
1
0
-0.4
-0.3
-0.2
-0.1
0
0.1
0.2
0.3
0.4

Figure 10(b)

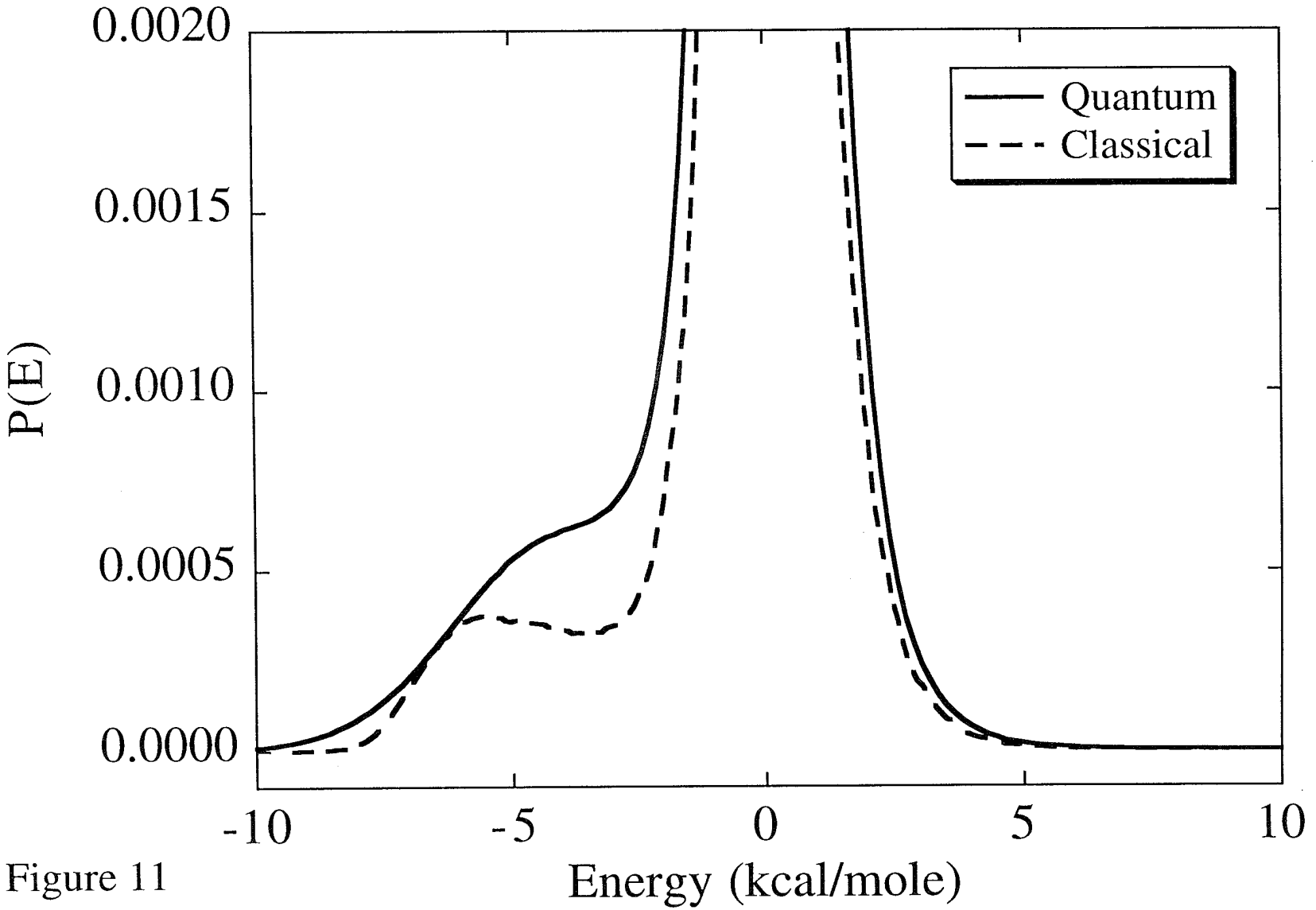
0.0020
0.0015
0.0010
0.0005
0.0000
P(E)
-10
-5
0
5
10
Energy (kcal/mole)
Quantum
Classical

Figure 11

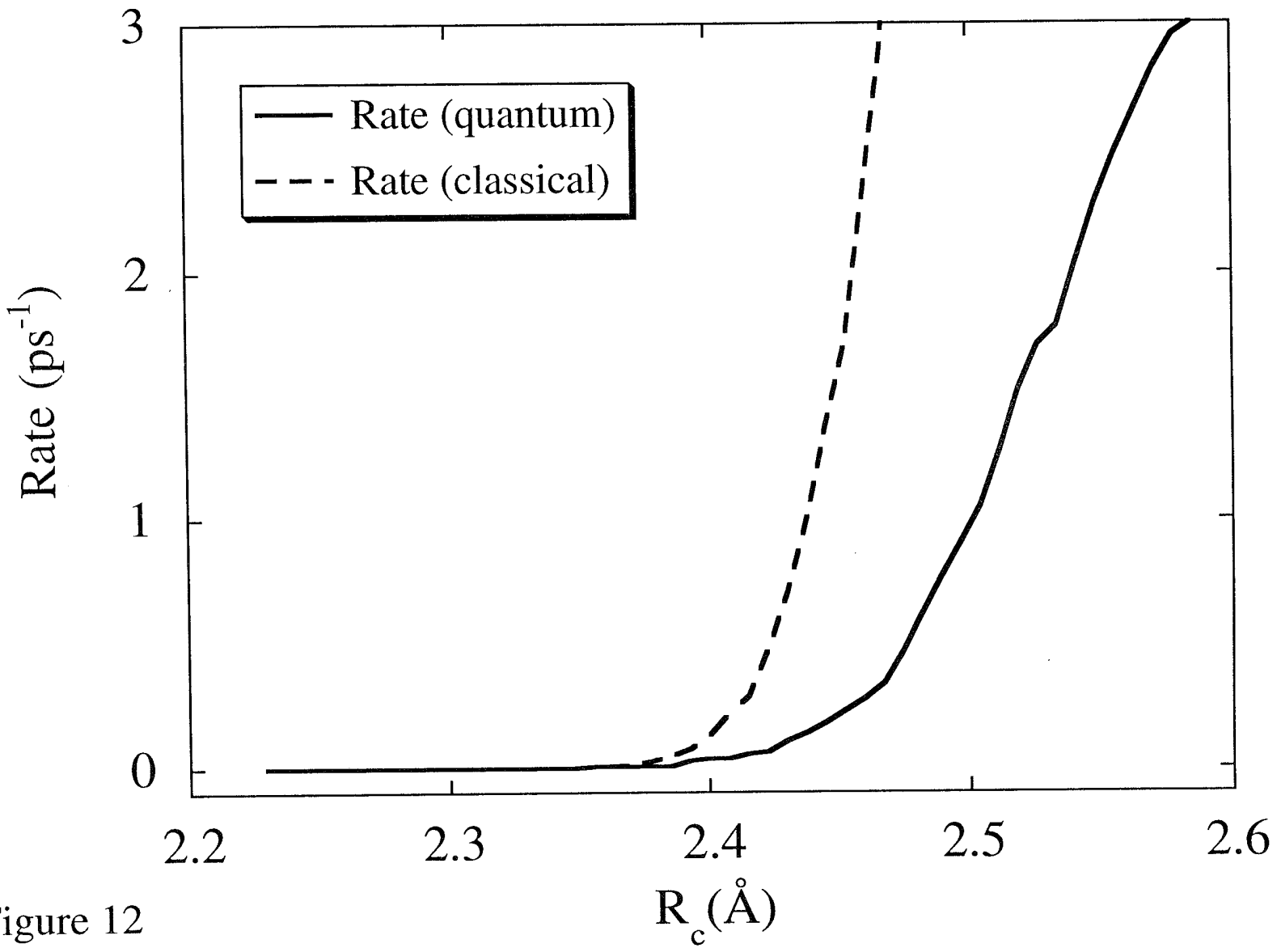


Figure 12

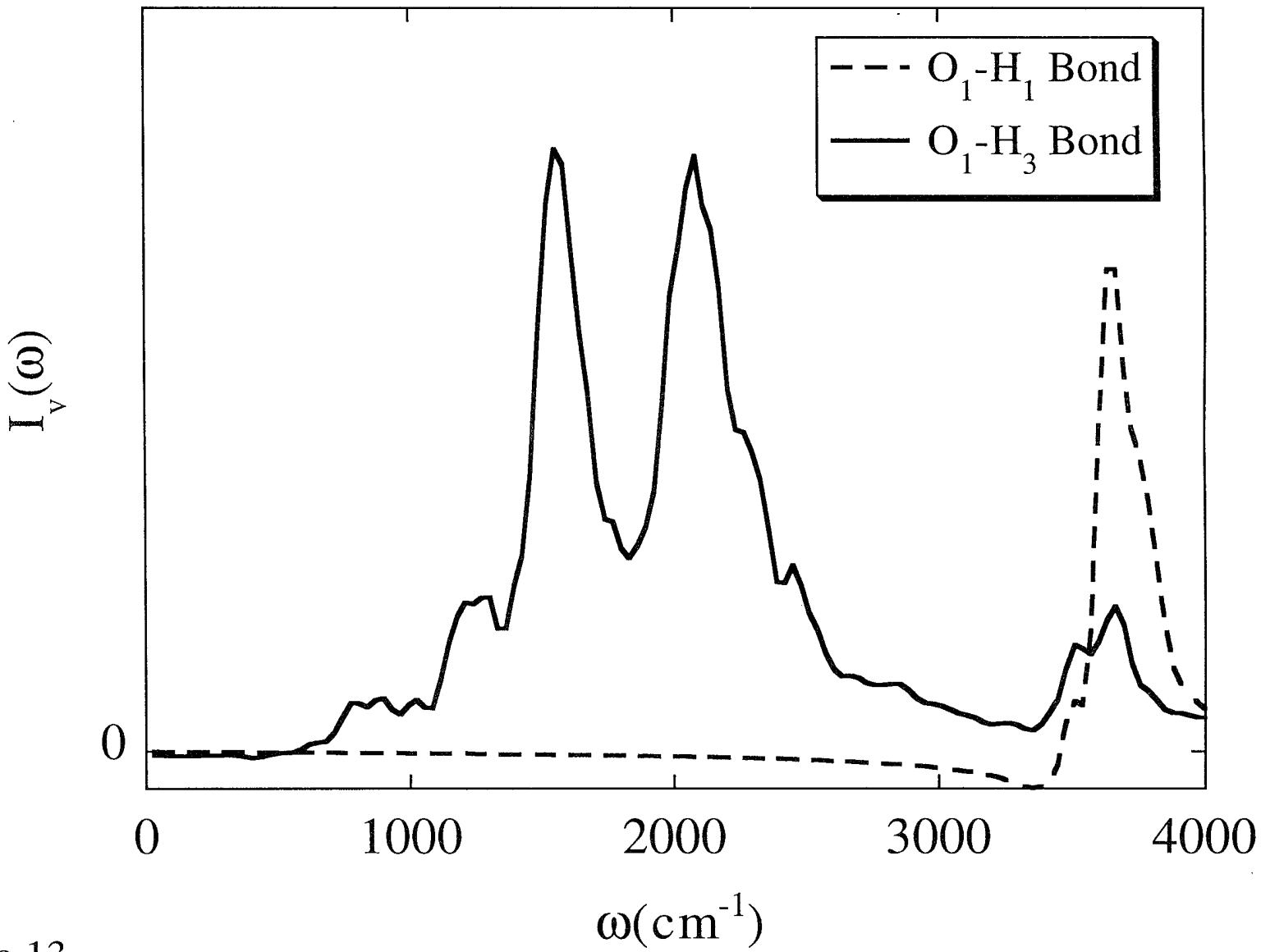


Figure 13